

FORTRESS: FORTRAN programs for solving coupled Gross-Pitaevskii equations for spin-orbit coupled spin-1 Bose-Einstein condensate

Pardeep Kaur^a, Arko Roy^b, Sandeep Gautam^{a,*}

^a*Department of Physics, Indian Institute of Technology Ropar, Rupnagar, Punjab 140001, India*

^b*INO-CNR BEC Center and Dipartimento di Fisica, Università di Trento, 38123 Trento, Italy*

Abstract

Here, we present simple and efficient numerical scheme to study static and dynamic properties of spin-1 Bose-Einstein condensates (BECs) with spin-orbit (SO) coupling by solving three coupled Gross-Pitaevskii equations (CGPEs) in three-, quasi-two and quasi-one dimensional systems. We provide a set of three codes developed in FORTRAN 90/95 programming language with user defined 'option' of imaginary and real-time propagation. We present the numerical results for energy, chemical potentials, and component densities for the ground state and compare with the available results from the literature. The results are presented for both the ferromagnetic and antiferromagnetic spin-1 BECs with and without SO coupling. To improve the computational speed, all the codes have the option of OpenMP parallelization. We have also presented the results for speedup and efficiency of OpenMP parallelization for the three codes with both imaginary and real-time propagation.

Keywords: Spin-1 BEC, Spin-orbit coupling, Time-splitting spectral method

PROGRAM SUMMARY

Program Title: FORTRESS

Licensing provisions: MIT

Programming language: (OpenMP) FORTRAN 90/95

Computer: Intel(R) Xeon(R) Platinum 8180 CPU @ 2.50GHz

Operating system: General

RAM: Will depend on array sizes.

Number of processors used: (OPENMP.THREADS used) 1 for serial and 8 with OpenMP in case of 1D code; 8 processors for 2D code, 16 processors for 3D code

External routines/libraries: FFTW 3.3.8

Journal reference of previous version: None

Nature of problem: To solve the coupled Gross-Pitaevskii equations for spin-1 BEC with anisotropic spin-orbit coupling using the time-splitting spectral method.

Solution method: We use the time-splitting Fourier spectral method to solve the coupled Gross-Pitaevskii equations. The resulting equations are evolved in imaginary time to obtain the ground state of the system

*Corresponding author.

E-mail address: pardeepmakkar23@gmail.com, arko.roy@unitn.it, sandeep@iitrpr.ac.in

Preprint submitted to Computer Physics Communications

or in real-time to study the dynamics.

1. Introduction

Over the past few decades, the study on cold dilute atomic gases has grown immensely since the experimental realization of Bose-Einstein condensation of bosonic gases in 1995 [1], a remarkable milestone in the field of ultracold atoms. In these early experiments [1], magnetic traps were used giving rise to scalar Bose-Einstein condensate (BEC) having frozen spin degrees of freedom. Optical traps on the other hand can trap all the hyperfine spin states of spin- f ultracold bosonic gas with f as the total spin per atom [2]. The advent of these optical traps led to the experimental realization of $2f + 1$ component Bose-Einstein condensates (BECs), corresponding to spin projection quantum number $m_f = -f, -f+1, \dots, +f$, and is known as spinor-BECs having $f = 1, 2$ and 3 [3]. Unlike most of the solid-state materials, in which spin-orbit (SO) coupling originates due to the relativistic effects, there was no spin-orbit coupling in the spinor BECs in this early set of experiments [3]. However, SO coupling can be engineered in spinor BECs by controlling the atom-light interaction leading to the generation of artificial non-Abelian Gauge potentials coupled to the atoms [4]. SO coupling was first engineered in a BEC of ^{87}Rb [5] by dressing two of its internal spin states from within the ground electric manifold ($5S_{1/2}, f = 1$) with a pair of lasers giving rise to equal strengths of Rashba [6] and Dresselhaus [7] terms which has attracted a lot of interest on experimental [8] and theoretical fronts [9, 10, 11]. SO coupling plays a key role in exotic phenomenon like spin-Hall effect [12], topological insulators [13] and has motivated new developments in spintronic devices [14], hybrid structures [15], and topological quantum computation [16], etc. Being highly tunable system and offering an unprecedented level of control, SO-coupled BEC has become an ideal quantum simulator to study these fascinating SO-coupled systems. More recently, SO coupling has been realized experimentally in spin-1 ^{87}Rb [17] which has stimulated more theoretical [18] and experimental [19] investigations. In the domain of strongly correlated electronic systems, recently, SO coupling has been employed to drive metal-insulator transition [20].

To describe a spin-1 BEC, the mean-field theory was developed independently by Ho [21] and Ohmi *et al.* [22]. In mean-field approximation, an SO-coupled spin-1 BEC is described by a set of three coupled time dependent nonlinear partial differential equations with first order derivative in time and first and second order derivatives in space [9]. Since there is no general analytic approach to solve a set of coupled Gross-Pitaevskii equations (CGPEs), one needs to solve the equations numerically, and this has spurred many studies on the numerical solutions of spin-1 BEC [23, 24, 25]. A wide range of numerical techniques have been employed in literature to study single component scalar [26, 27, 28, 29, 30, 31], multicomponent scalar [32] as well as spinor BECs [23, 24, 25, 33]. One of the most widely used method to determine the ground state of a scalar BECs is the imaginary time method followed by an appropriate discretization scheme to evolve the resultant gradient flow equations [27, 28]. The extension of this method to compute the ground states of spin-1 BEC is not straightforward, as there are only two constraints, i.e. the conservation of total number of atoms and longitudinal magnetization, while one would need three projection parameters for normalization of three components of wavefunction [23, 24, 25]. However, imaginary time method has been used in the literature with the simultaneous conservation of norm and magnetization achieved through the introduction of the third normalization condition [23, 24, 25]. There have been different discretization schemes used which include, among others, centered finite difference scheme and spectral methods for spatial discretization

and forward Euler, backward Euler, and Crank-Nicolson schemes for time discretization. The non-linear terms can be handled easily by first using the time-splitting technique, which in the case of scalar Gross-Pitaevskii (GP) equation amounts to approximating the solution by successively solving two equations- one of which is just a free particle Schrödinger equation, and the other containing the non-linear term can be solved exactly [29]. The free particle Schrödinger equation can be handled by Crank-Nicolson [30] or spectral discretization [31, 34]. In the present work, we use the Fourier spectral discretization for solving the free particle Schrödinger equation. A couple of advantages of choosing this method: firstly it can be extended easily to the higher dimensional systems because of the ease of dealing with the differential operators in Fourier space, and secondly its spectral accuracy. It is worth pointing out here that even with growing number of experimental and theoretical investigations related to SO-coupled spin-1 BECs, the technical details of dealing with SOC terms from the numerical point of view is still lacking in the literature. This sets the motivation for this current work. There are numerous software packages written in different programming languages (C, C++, FORTRAN, MATLAB, etc.) to deal with solving single or two-coupled GP equations, with and without dipolar interactions, under rotating traps, etc. [35]. However, to the best of our knowledge, packages dealing with SO coupled spin-1 BEC are unavailable. We make here an attempt to bridge this gap, and make our codes general enough to include (a) anisotropic SO coupling, (b) explicit Rashba or Dresselhaus type of coupling, or (c) mixture of both. Each of the three codes has the option of *imaginary-time* and *real-time* propagation to be chosen by the user. The purpose of imaginary-time propagation, which is also referred to as normalized gradient flow method [24, 25], is to find the stationary state solutions of the system, whereas the real-time propagation allows the user to study the real-time dynamics. We use imaginary time propagation to find the ground state solutions of SO-coupled quasi-one-dimensional (q1D), quasi-two-dimensional (q2D) and three-dimensional (3D) spin-1 BECs.

We use the time-splitting technique [23, 29, 30] to split the CGPEs into four sets of equations where each set (consisting of three equations) is amenable to be numerically solvable by an appropriate method. These four sets of equations are solved successively as per the standard Lie-splitting prescription, which is first order accurate in time for two non-commuting operators. If the solution of the CGPEs is known at time t , say $\Phi(t)$, then Lie splitting approximates the solution of the CGPEs at time $t + \delta t$ with the solution obtained by successively solving the aforementioned four sets of equations, wherein the solution to each set serves as the initial (transient) solution for the following set; except for the first set of equations, whose initial solution is $\Phi(t)$. We term the method described above as time-splitting real-time propagation [23, 29, 30]. To calculate the ground state solutions, we use imaginary-time propagation [23, 24, 25] which takes any initial guess to the ground state wavefunction after sufficiently large number of time steps; as is expected, the number of time steps needed to obtain a converged ground state solution depends crucially on the initial guess.

The main focus of the present paper is to provide efficient and easy to implement numerical scheme to solve the CGPEs with anisotropic SO coupling [9] in imaginary time or real-time. We have implemented the numerical scheme via a set of FORTRAN 90/95 codes which can be easily used by the students and the researchers working on SO coupled spin-1 BECs. We have used harmonic potentials for trapped systems which is widely used in experiments, nonetheless the use of Fourier spectral technique makes the codes ideal to study the homogeneous system, which is pertinent in the context of the experimental realization of the box trapping potential [36]. We present the results for energy, chemical potentials and densities of ground state wave functions obtained with the codes and compare them with the earlier reported results in the

literature [24, 25].

The paper is organized as follows. In section 2, we describe the mean-field CGPEs with SO coupling for spin-1 condensate, and then the dimensionless formulation of these equations in three dimension. This is followed by the reduction of the set for q2D and q1D BECs. In section 3, we discuss the details of the numerical approach to solve these equations in one dimension, followed by the discussion on q2D and 3D spinor BECs. For the sake of brevity, in q2D and 3D cases, the emphasis of the discussion is on the additional changes to the q1D scheme. We conclude the section with a discussion on discretization scheme in real and Fourier space for sake of completeness. In section 4, we present the description of FORTRAN programs which include definition of the various data variables or constant parameters and the functions of the various subroutines. In section 5, we present the results for performance parameters like speedup and efficiency of OpenMP programs for both imaginary and real-time propagations. In section 6, we present the results for energy, chemical potentials, component wave-functions or densities and compare them with the ones reported by other researchers.

2. Coupled Gross-Pitaevskii equations for spin-orbit coupled BEC

In 3D case, the single particle Hamiltonian of spin-1 BEC in the presence of anisotropic [6, 37] SO coupling is given by [9, 10]

$$H_0 = \frac{p_x^2 + p_y^2 + p_z^2}{2m} + \gamma_x p_x \Sigma_x + \gamma_y p_y \Sigma_y + \gamma_z p_z \Sigma_z, \quad (1)$$

where $p_x = -i\hbar\partial/\partial x$, $p_y = -i\hbar\partial/\partial y$, and $p_z = -i\hbar\partial/\partial z$ correspond to the momentum operators along x , y and z directions, respectively. Also, m is the mass of each atom and Σ_x , Σ_y , and Σ_z are the irreducible matrix representations of the x , y and z components of the spin-1 angular momentum operator, respectively, which are given by

$$\Sigma_x = \frac{1}{\sqrt{2}} \begin{pmatrix} 0 & 1 & 0 \\ 1 & 0 & 1 \\ 0 & 1 & 0 \end{pmatrix}, \quad \Sigma_y = \frac{1}{\sqrt{2}i} \begin{pmatrix} 0 & 1 & 0 \\ -1 & 0 & 1 \\ 0 & -1 & 0 \end{pmatrix}, \quad \Sigma_z = \begin{pmatrix} 1 & 0 & 0 \\ 0 & 0 & 0 \\ 0 & 0 & -1 \end{pmatrix}, \quad (2)$$

where γ_x , γ_y , and γ_z are the strengths of SO coupling. In standard isotropic SO coupling, $\gamma_x = \gamma_y = \gamma_z = \hbar k_r/m$ realized by using two counter-propagating Raman lasers of wavelength λ_r aligned at an angle β_r and k_r is given by $k_r = (2\pi \sin \beta_r/2)/\lambda_r$.

For weakly interacting SO-coupled spin-1 BEC, the properties of system are well described under mean-field approximation by the following coupled Gross-Pitaevskii equations (CGPEs) [9, 21, 22, 23]

$$i\hbar \frac{\partial \psi_1}{\partial t} = \mathcal{H}\psi_1 + c_2(\rho_0 + \rho_-)\psi_1 + c_2\psi_{-1}^*\psi_0^2 - \frac{i\hbar}{\sqrt{2}} \left(\gamma_x \frac{\partial \psi_0}{\partial x} - i\gamma_y \frac{\partial \psi_0}{\partial y} + \sqrt{2}\gamma_z \frac{\partial \psi_1}{\partial z} \right), \quad (3a)$$

$$i\hbar \frac{\partial \psi_0}{\partial t} = \mathcal{H}\psi_0 + c_2\rho_+\psi_0 + 2c_2\psi_1\psi_{-1}\psi_0^* - \frac{i\hbar}{\sqrt{2}} \left[\gamma_x \left(\frac{\partial \psi_1}{\partial x} + \frac{\partial \psi_{-1}}{\partial x} \right) + i\gamma_y \left(\frac{\partial \psi_1}{\partial y} - \frac{\partial \psi_{-1}}{\partial y} \right) \right] \quad (3b)$$

$$i\hbar \frac{\partial \psi_{-1}}{\partial t} = \mathcal{H}\psi_{-1} + c_2(\rho_0 - \rho_-)\psi_{-1} + c_2\psi_1^*\psi_0^2 - \frac{i\hbar}{\sqrt{2}} \left(\gamma_x \frac{\partial \psi_0}{\partial x} + i\gamma_y \frac{\partial \psi_0}{\partial y} - \sqrt{2}\gamma_z \frac{\partial \psi_{-1}}{\partial z} \right), \quad (3c)$$

where

$$\mathcal{H} = \left(-\frac{\hbar^2}{2m}\nabla^2 + V(\mathbf{x}) + c_0\rho\right), \quad \mathbf{x} = (x, y, z), \quad (4)$$

and $\Psi = (\psi_1(\mathbf{x}, t), \psi_0(\mathbf{x}, t), \psi_{-1}(\mathbf{x}, t))^T$ with ψ_1, ψ_0 and ψ_{-1} as the component wavefunctions, and $V(\mathbf{x}) = m(\omega_x^2 x^2 + \omega_y^2 y^2 + \omega_z^2 z^2)/2$ is 3D harmonic trap. Also,

$$c_0 = \frac{4\pi\hbar^2(a_0 + 2a_2)}{3m}, \quad c_2 = \frac{4\pi\hbar^2(a_2 - a_0)}{3m}, \quad \nabla^2 = \frac{\partial^2}{\partial x^2} + \frac{\partial^2}{\partial y^2} + \frac{\partial^2}{\partial z^2}, \quad (5)$$

where a_0 and a_2 correspond to the s -wave scattering lengths in total spin 0 and 2 channels, respectively; ω_x, ω_y and ω_z are the confining trap frequencies along x, y and z directions, respectively; $\rho_{\pm} = \rho_{+1} \pm \rho_{-1}$ where $\rho_j = |\psi_j|^2$ with $j = 1, 0, -1$ are the component densities and $\rho = \sum_{j=-1}^1 |\psi_j|^2$ is the total density.

2.1. Important conserved quantities of Spin-1 BEC

Three important conserved quantities of spin-1 BEC are total number of particles N , longitudinal magnetization \mathcal{M} (which is conserved on the time scale of spin-1 BEC experiments), and total energy E . These are given as

$$N = \int_{-\infty}^{\infty} d\mathbf{x} \sum_{j=-1}^1 |\psi_j(\mathbf{x})|^2, \quad (6a)$$

$$\mathcal{M} = \sum_{j=-1}^1 \int j |\psi_j(\mathbf{x}, t)|^2 d\mathbf{x}, \quad (6b)$$

$$\begin{aligned} E = & \int d\mathbf{x} \left[\sum_{j=-1}^1 \psi_j^* \left(-\frac{\hbar^2 \nabla^2}{2m} + V \right) \psi_j + \frac{c_0}{2} \rho^2 + \frac{c_2}{2} (\rho_1 + \rho_0 - \rho_{-1}) \rho_1 + \frac{c_2}{2} (\rho_0 + \rho_{-1} - \rho_1) \rho_{-1} \right. \\ & + c_2 (\psi_{-1}^* \psi_0^2 \psi_1^* + \psi_{-1} \psi_0^{2*} \psi_1) + \frac{c_2}{2} (\rho_1 + \rho_{-1}) \rho_0 - \frac{i\hbar\gamma_x}{\sqrt{2}} \psi_0^* \left(\frac{\partial\psi_1}{\partial x} + \frac{\partial\psi_{-1}}{\partial x} \right) \\ & + \frac{\hbar}{\sqrt{2}} \psi_0^* \left(\gamma_y \frac{\partial\psi_1}{\partial y} - \gamma_x \frac{\partial\psi_{-1}}{\partial x} \right) - \frac{i\hbar\gamma_x}{\sqrt{2}} (\psi_1^* + \psi_{-1}^*) \frac{\partial\psi_0}{\partial x} - \frac{\hbar\gamma_y}{\sqrt{2}} (\psi_1^* - \psi_{-1}^*) \frac{\partial\psi_0}{\partial y} \\ & \left. - i\hbar\gamma_z \left(\psi_1^* \frac{\partial\psi_1}{\partial z} - \psi_{-1}^* \frac{\partial\psi_{-1}}{\partial z} \right) \right]. \quad (7) \end{aligned}$$

2.2. Chemical potential

For stationary states, the wavefunctions have the trivial time dependence $\psi_j(\mathbf{x}, t) = e^{-i\mu_j t} \psi_j(\mathbf{x})$ through the Madelung transformation. By plugging this into Eqs. (3a)-(3c), the time independent CGPEs are

$$\mu_1 \psi_1 = [\mathcal{H} + c_2(\rho_0 + \rho_{-})] \psi_1 + c_2 \psi_{-1}^* \psi_0^2 - \frac{i\hbar}{\sqrt{2}} \left(\gamma_x \frac{\partial\psi_0}{\partial x} - i\gamma_y \frac{\partial\psi_0}{\partial y} + \sqrt{2}\gamma_z \frac{\partial\psi_1}{\partial z} \right), \quad (8a)$$

$$\mu_0 \psi_0 = [\mathcal{H} + c_2 \rho_+] \psi_0 + 2c_2 \psi_0^* \psi_1 \psi_{-1} - \frac{i\hbar}{\sqrt{2}} \left(\gamma_x \frac{\partial\psi_1}{\partial x} + i\gamma_y \frac{\partial\psi_1}{\partial y} + \gamma_x \frac{\partial\psi_{-1}}{\partial x} - i\gamma_y \frac{\partial\psi_{-1}}{\partial y} \right) \quad (8b)$$

$$\mu_{-1} \psi_{-1} = [\mathcal{H} + c_2(\rho_0 - \rho_{-})] \psi_{-1} + c_2 \psi_1^* \psi_0^2 - \frac{i\hbar}{\sqrt{2}} \left(\gamma_x \frac{\partial\psi_0}{\partial x} + i\gamma_y \frac{\partial\psi_0}{\partial y} - \sqrt{2}\gamma_z \frac{\partial\psi_{-1}}{\partial z} \right), \quad (8c)$$

where μ_1, μ_0 and μ_{-1} are the chemical potentials of the three components. These equations can be used to define the chemical potential functionals analogous to energy functional.

2.3. Dimensionless formulation of 3D CGPEs

Eqs. (3a) - (3c) can be transformed into dimensionless form by introducing the following dimensionless variables

$$\tilde{t} = 2\omega_x t, \quad \tilde{\mathbf{x}} = \frac{\mathbf{x}}{a_{\text{osc}}}, \quad \phi_j(\tilde{\mathbf{x}}, \tilde{t}) = \frac{a_{\text{osc}}^{3/2}}{\sqrt{N}} \psi_j(\tilde{\mathbf{x}}, \tilde{t}), \quad a_{\text{osc}} = \sqrt{\frac{\hbar}{m\omega_x}} \quad (9)$$

where a_{osc} is the oscillator length. This basically fixes the units of length, time, density, and energy as a_{osc} , $1/2\omega_x$, a_{osc}^{-3} , and $\hbar\omega_x$, respectively. After substitution of these new parameters and removing all tildes for notational simplicity, we get the following dimensionless CGPEs in 3D [23, 38]

$$i \frac{\partial \phi_1}{\partial t} = \mathcal{H}\phi_1 + 2c_2(\rho_0 + \rho_-)\phi_1 + 2c_2\phi_{-1}^*\phi_0^2 - \sqrt{2}i \left(\gamma_x \frac{\partial \phi_0}{\partial x} - i\gamma_y \frac{\partial \phi_0}{\partial y} + \sqrt{2}\gamma_z \frac{\partial \phi_1}{\partial z} \right), \quad (10a)$$

$$i \frac{\partial \phi_0}{\partial t} = \mathcal{H}\phi_0 + 2c_2\rho_+\phi_0 + 4c_2\phi_1\phi_{-1}\phi_0^* - \sqrt{2}i \left(\gamma_x \frac{\partial \phi_1}{\partial x} + i\gamma_y \frac{\partial \phi_1}{\partial y} + \gamma_x \frac{\partial \phi_{-1}}{\partial x} - i\gamma_y \frac{\partial \phi_{-1}}{\partial y} \right), \quad (10b)$$

$$i \frac{\partial \phi_{-1}}{\partial t} = \mathcal{H}\phi_{-1} + 2c_2(\rho_0 - \rho_-)\phi_{-1} + 2c_2\phi_1^*\phi_0^2 - \sqrt{2}i \left(\gamma_x \frac{\partial \phi_0}{\partial x} + i\gamma_y \frac{\partial \phi_0}{\partial y} - \sqrt{2}\gamma_z \frac{\partial \phi_{-1}}{\partial z} \right), \quad (10c)$$

where

$$\mathcal{H} = -\nabla^2 + 2V(\mathbf{x}) + 2c_0\rho, \quad V(\mathbf{x}) = (\alpha_x^2 x^2 + \alpha_y^2 y^2 + \alpha_z^2 z^2)/2, \quad (11)$$

$\alpha_\eta = \omega_\eta/\omega_x$ with $\eta = x, y, z$ and new c_0, c_2 and γ are given by

$$c_0 = \frac{4\pi N(a_0 + 2a_2)}{3a_{\text{osc}}}, \quad c_2 = \frac{4\pi N(a_2 - a_0)}{3a_{\text{osc}}}, \quad \gamma_x = \gamma_y = \gamma_z = k_r a_{\text{osc}}. \quad (12)$$

Also, $\rho_j = |\phi_j|^2$ with $j = 1, 0, -1$ are the component densities, $\rho = \sum_{j=-1}^1 |\phi_j|^2$ is the total density, and now it is normalized to unity, i.e. $\int \rho d\mathbf{x} = 1$.

2.4. CGPEs for q2D Spin-1 BEC

If the trapping frequencies along any direction, let us say z is much larger than the geometric mean of frequencies along other two directions, i.e x and y , then $\alpha_x = 1$, $\alpha_y \approx 1$ and $\alpha_z \gg \alpha_x$ [23]. In this case, the dimensionless generalized CGPEs in 3D can be approximated by 2D equations by choosing [39]

$$\phi_j(x, y, z, t) = \phi_j(x, y, t)\phi_{\text{ho}}(z), \quad \phi_{\text{ho}}(z) = (\alpha_z/\pi)^{1/4} \exp(-\alpha_z z^2/2). \quad (13)$$

Generalized dimensionless CGPEs in 2D are given by [23, 40]

$$i \frac{\partial \phi_1}{\partial t} = \mathcal{H}\phi_1 + 2c_2(\rho_0 + \rho_-)\phi_1 + 2c_2\phi_{-1}^*\phi_0^2 - \sqrt{2}i \left(\gamma_x \frac{\partial \phi_0}{\partial x} - i\gamma_y \frac{\partial \phi_0}{\partial y} \right), \quad (14a)$$

$$i \frac{\partial \phi_0}{\partial t} = \mathcal{H}\phi_0 + 2c_2\rho_+\phi_0 + 4c_2\phi_1\phi_{-1}\phi_0^* - \sqrt{2}i \left(\gamma_x \frac{\partial \phi_1}{\partial x} + i\gamma_y \frac{\partial \phi_1}{\partial y} + \gamma_x \frac{\partial \phi_{-1}}{\partial x} - i\gamma_y \frac{\partial \phi_{-1}}{\partial y} \right), \quad (14b)$$

$$i \frac{\partial \phi_{-1}}{\partial t} = \mathcal{H}\phi_{-1} + 2c_2(\rho_0 - \rho_-)\phi_{-1} + 2c_2\phi_1^*\phi_0^2 - \sqrt{2}i \left(\gamma_x \frac{\partial \phi_0}{\partial x} + i\gamma_y \frac{\partial \phi_0}{\partial y} \right), \quad (14c)$$

where

$$\mathcal{H} = -\nabla_{xy}^2 + 2V(\mathbf{x}) + 2c_0\rho, \quad \nabla_{xy}^2 = \frac{\partial^2}{\partial x^2} + \frac{\partial^2}{\partial y^2}, \quad \mathbf{x} = (x, y). \quad (15)$$

The trapping potential $V(\mathbf{x})$ and interaction parameters c_0 and c_2 are now defined as

$$V(\mathbf{x}) = \frac{1}{2}(\alpha_x^2 x^2 + \alpha_y^2 y^2), \quad c_0 = \sqrt{\frac{\alpha_z}{2\pi}} \frac{4\pi N(a_0 + 2a_2)}{3a_{\text{osc}}}, \quad c_2 = \sqrt{\frac{\alpha_z}{2\pi}} \frac{4\pi N(a_2 - a_0)}{3a_{\text{osc}}}. \quad (16)$$

2.5. CGPEs for q1D Spin-1 BEC

If the trap is much stronger along two directions, say y and z compared to the x direction then $\alpha_x = 1, \alpha_y \gg \alpha_x, \alpha_z \gg \alpha_x$ then by assuming [39]

$$\phi_j(x, y, z, t) = \phi_j(x, t)\phi_{\text{ho}}(y, z), \quad \phi_{\text{ho}}(y, z) = (\sqrt{\alpha_y \alpha_z / \pi})^{1/2} \exp[-(\alpha_y y^2 + \alpha_z z^2)/2], \quad (17)$$

Eqs. (10a)-(10c) can be reduced into quasi-1D equations [23, 41]

$$i \frac{\partial \phi_1}{\partial t} = \mathcal{H}\phi_1 + 2c_2(\rho_0 + \rho_-)\phi_1 + 2c_2\phi_{-1}^*\phi_0^2 - \sqrt{2}i\gamma_x \left(\frac{\partial \phi_0}{\partial x} \right), \quad (18a)$$

$$i \frac{\partial \phi_0}{\partial t} = \mathcal{H}\phi_0 + 2c_2\rho_+\phi_0 + 4c_2\phi_1\phi_{-1}\phi_0^* - \sqrt{2}i\gamma_x \left(\frac{\partial \phi_1}{\partial x} + \frac{\partial \phi_{-1}}{\partial x} \right), \quad (18b)$$

$$i \frac{\partial \phi_{-1}}{\partial t} = \mathcal{H}\phi_{-1} + 2c_2(\rho_0 - \rho_-)\phi_{-1} + 2c_2\phi_1^*\phi_0^2 - \sqrt{2}i\gamma_x \left(\frac{\partial \phi_0}{\partial x} \right), \quad (18c)$$

where

$$\begin{aligned} \mathcal{H} &= -\frac{\partial^2}{\partial x^2} + 2V(x) + 2c_0\rho, \quad V(x) = \frac{1}{2}\gamma_x^2 x^2, \\ c_0 &= \frac{\sqrt{\alpha_y \alpha_z}}{2\pi} \frac{4\pi N(a_0 + 2a_2)}{3a_{\text{osc}}}, \quad c_2 = \frac{\sqrt{\alpha_y \alpha_z}}{2\pi} \frac{4\pi N(a_2 - a_0)}{3a_{\text{osc}}}. \end{aligned}$$

3. Numerical Methods

3.1. Solution of q1D CGPEs

Starting with the simplest case of q1D spin-1 BEC, Eqs (18a)-(18c) can be written in simplified form as

$$i \frac{\partial \Phi}{\partial t} = \mathbf{H}\Phi. \quad (19)$$

Here, $\Phi = (\phi_1, \phi_0, \phi_{-1})^T$ and Hamiltonian \mathbf{H} consists of different terms involving kinetic energy operator H_{KE} , trapping potential plus terms resulting from spin-preserving collisions H_{SP} , terms corresponding to spin-exchange collisions H_{SE} , and spin-orbit coupling H_{SOC} . Eq. (19) can then be written as

$$i \frac{\partial \Phi}{\partial t} = (H_{\text{KE}} + H_{\text{SP}} + H_{\text{SE}} + H_{\text{SOC}})\Phi, \quad (20)$$

where $H_{\text{KE}}, H_{\text{SP}}, H_{\text{SE}}$ and H_{SOC} are 3×3 matrix operators defined as

$$H_{\text{KE}} = \begin{pmatrix} -\partial_{xx} & 0 & 0 \\ 0 & -\partial_{xx} & 0 \\ 0 & 0 & -\partial_{xx} \end{pmatrix}, \quad H_{\text{SOC}} = -\sqrt{2}i\gamma_x \begin{pmatrix} 0 & \partial_x & 0 \\ \partial_x & 0 & \partial_x \\ 0 & \partial_x & 0 \end{pmatrix}, \quad (21a)$$

$$H_{SE} = \begin{pmatrix} 0 & 2c_2\phi_0\phi_{-1}^* & 0 \\ 2c_2\phi_0^*\phi_{-1} & 0 & 2c_2\phi_0^*\phi_1 \\ 0 & 2c_2\phi_0\phi_1^* & 0 \end{pmatrix}, \quad (21b)$$

$$H_{SP} = 2 \begin{pmatrix} V + c_0\rho + c_2(\rho_0 + \rho_-) & 0 & 0 \\ 0 & V + c_0\rho + c_2\rho_+ & 0 \\ 0 & 0 & V + c_0\rho + c_2(\rho_0 - \rho_-) \end{pmatrix}. \quad (21c)$$

To solve these equations (20), we use operator splitting which has been extensively used in the numerical solutions of non-linear Schrödinger equation including GP equation [30, 42] and coupled GP equations [23]. Here, we have used first order time splitting known as Lie splitting.

Solution to Eq. (20) after time step δt is given as

$$\Phi(t + \delta t) = \hat{U}\Phi(t), \quad (22)$$

which describes the evolution of the wave function by a unitary propagator \hat{U} given as

$$\hat{U} = \exp[-i\delta t(H_{SP} + H_{SE} + H_{SOC} + H_{KE})], \quad (23)$$

The propagator can be approximated by split operator technique as

$$\hat{U} \approx \exp(-i\delta t H_{SP}) \exp(-i\delta t H_{SE}) \exp(-i\delta t H_{SOC}) \exp(-i\delta t H_{KE}). \quad (24)$$

Using (24), Eq. (22) is equivalent to solving following equations successively

$$i\frac{\partial\Phi}{\partial t} = H_{KE}\Phi, \quad (25a)$$

$$i\frac{\partial\Phi}{\partial t} = H_{SOC}\Phi, \quad (25b)$$

$$i\frac{\partial\Phi}{\partial t} = H_{SE}\Phi, \quad (25c)$$

$$i\frac{\partial\Phi}{\partial t} = H_{SP}\Phi. \quad (25d)$$

Eq. (25a) can be written as the following set of decoupled equations

$$i\frac{\partial\phi_j(x,t)}{\partial t} = -\frac{\partial^2\phi_j(x,t)}{\partial x^2}, \quad j = -1, 0, 1. \quad (26)$$

Solution of Eq. (26) in Fourier space is given as

$$\hat{\phi}_j(k_x, t + \delta t) = \hat{\phi}_j(k_x, t) \exp(-ik_x^2\delta t), \quad (27)$$

where $\hat{\phi}_j$ is the Fourier transform of ϕ_j and k_x is known as Fourier frequency. Now, $\hat{\phi}_j(k_x, t + \delta t)$, transient wavefunction in Fourier space, is the initial value of wavefunction for the Fourier transform of Eq. (25b), i.e.,

$$i\frac{\partial\hat{\Phi}(k_x, t)}{\partial t} = \hat{H}_{SOC}\hat{\Phi}(k_x, t). \quad (28)$$

Here \hat{H}_{SOC} is given as

$$\hat{H}_{SOC} = -\sqrt{2}i\gamma_x \begin{pmatrix} 0 & ik_x & 0 \\ ik_x & 0 & ik_x \\ 0 & ik_x & 0 \end{pmatrix}, \quad (29)$$

and $\hat{\Phi}(k_x, t)$ is the Fourier transforms of $\Phi(x, t)$. The solution of equation (28) is given as [38, 40]

$$\begin{aligned}\hat{\Phi}(k_x, t + \delta t) &= e^{-i\hat{H}_{\text{SOC}}\delta t}\hat{\Phi}(k_x, t) = e^{-i\hat{G}}\hat{\Phi}(k_x, t) \\ &= \left(I + \frac{\cos\beta - 1}{\beta^2}\hat{G}^2 - i\frac{\sin\beta}{\beta}\hat{G} \right)\hat{\Phi}(k_x, t),\end{aligned}\quad (30)$$

where $\beta = \sqrt{2}A\delta t$ with $A = \sqrt{2}\gamma_x k_x$ and \hat{G} is defined as

$$\hat{G} = \delta t \begin{pmatrix} 0 & A & 0 \\ A & 0 & A \\ 0 & A & 0 \end{pmatrix}. \quad (31)$$

Wavefunction in Eq. (30) is in Fourier space and is inverse Fourier transformed to obtain the transient wavefunction in co-ordinate space which serves as the initial solution for Eq. (25c). The solution of Eq. (25c) is now given by

$$\begin{aligned}\Phi(x, t + \delta t) &= e^{-iH_{\text{SE}}\delta t}\Phi(x, t) = e^{-i\hat{O}}\Phi(x, t) \\ &= \left(I + \frac{\cos\Omega - 1}{\Omega^2}\hat{O}^2 - i\frac{\sin\Omega}{\Omega}\hat{O} \right)\Phi(x, t)\end{aligned}\quad (32)$$

where H_{SE} is given in Eq. (21b) and \hat{O} is defined as

$$\hat{O} = \delta t \begin{pmatrix} 0 & A & 0 \\ A^* & 0 & B^* \\ 0 & B & 0 \end{pmatrix}. \quad (33)$$

with $\Omega = \delta t \sqrt{|A|^2 + |B|^2}$, $A = 2c_2\phi_0\phi_{-1}^*$ and $B = 2c_2\phi_0\phi_1^*$

The transient wave function we get from here is in configuration space and is used as an input wavefunction for remaining Eq. (25d). H_{SP} being diagonal, the solution to Eq. (25d) can be calculated analytically as

$$\Phi(x, t + \delta t) = \exp(-i\delta t H_{\text{SP}})\Phi(x, t). \quad (34)$$

This final wavefunction is solution of Eq. (22) after time δt .

3.1.1. Solution of q2D CGPEs

The method discussed in previous subsection can be extended to q2D and 3D systems with some modifications which we will elaborate in the rest of this section. In q2D spin-1 BECs, Eqs. (14a)-(14c) can again be written in simplified form as Eq. (19). Here too H can be considered as consisting of, aptly defined, H_{KE} , H_{SOC} , H_{SE} and H_{SP} . Now, H_{KE} and H_{SOC} for q2D SO-coupled BECs are given as

$$H_{\text{KE}} = \begin{pmatrix} -\nabla_{xy}^2 & 0 & 0 \\ 0 & -\nabla_{xy}^2 & 0 \\ 0 & 0 & -\nabla_{xy}^2 \end{pmatrix}, \quad (35a)$$

$$H_{\text{SOC}} = -\sqrt{2}i \begin{pmatrix} 0 & \gamma_x\partial_x - i\gamma_y\partial_y & 0 \\ \gamma_x\partial_x + i\gamma_y\partial_y & 0 & \gamma_x\partial_x - i\gamma_y\partial_y \\ 0 & \gamma_x\partial_x + i\gamma_y\partial_y & 0 \end{pmatrix}, \quad (35b)$$

whereas H_{SE} and H_{SP} are again defined by Eqs. (21b) and (21c), respectively, where V , c_0 and c_2 are now given by Eq. (16). Again as in q1D systems, solution of Eqs. (14a)-(14c) is approximated by solving Eqs. (25a)-(25d) successively. Solution to Eq. (25a) with H_{KE} defined by Eq. (35a) in this case is given in Fourier space as

$$\hat{\phi}_j(k_x, k_y, t + \delta t) = \hat{\phi}_j(k_x, k_y, t) \exp[-i(k_x^2 + k_y^2)\delta t]. \quad (36)$$

Fourier transform of Eq. (25b) corresponding to H_{SOC} given by Eq. (35b) is given as

$$\frac{i\partial\hat{\Phi}(k_x, k_y, t)}{\partial t} = \hat{H}_{SOC}\hat{\Phi}(k_x, k_y, t), \quad (37)$$

where \hat{H}_{SOC} in Fourier space is given as

$$\hat{H}_{SOC} = -\sqrt{2}i \begin{pmatrix} 0 & i\gamma_x k_x + \gamma_y k_y & 0 \\ i\gamma_x k_x - \gamma_y k_y & 0 & i\gamma_x k_x + \gamma_y k_y \\ 0 & i\gamma_x k_x - \gamma_y k_y & 0 \end{pmatrix}. \quad (38)$$

Solution to (37) is given as [38, 40]

$$\begin{aligned} \hat{\Phi}(k_x, k_y, t + \delta t) &= e^{-i\hat{H}_{SOC}\delta t}\hat{\Phi}(k_x, k_y, t) = e^{-i\hat{G}}\hat{\Phi}(k_x, k_y, t) \\ &= \left(I + \frac{\cos\beta - 1}{\beta^2}\hat{G}^2 - i\frac{\sin\beta}{\beta}\hat{G} \right) \hat{\Phi}(k_x, k_y, t), \end{aligned} \quad (39)$$

where $\beta = \sqrt{2}|A|\delta t$, $A = \sqrt{2}(\gamma_x k_x - i\gamma_y k_y)$, $A^* = \sqrt{2}(\gamma_x k_x + i\gamma_y k_y)$ and \hat{G} is defined as

$$\hat{G} = \delta t \begin{pmatrix} 0 & A & 0 \\ A^* & 0 & A \\ 0 & A^* & 0 \end{pmatrix}. \quad (40)$$

Eqs. (25c) and (25d) are solved similarly as in q1D case.

3.1.2. Solutions of 3D CGPEs

In 3D case too, forms of H_{SE} and H_{SP} are same as defined in (21b) and (21c) where $V(\mathbf{x})$, c_0 and c_2 are defined in Eqs. (11)-(12) allowing us to use the methods discussed in q1D case to solve Eqs. (25c)-(25d). On the other hand, H_{KE} and H_{SOC} are given as

$$H_{KE} = \begin{pmatrix} -\nabla^2 & 0 & 0 \\ 0 & -\nabla^2 & 0 \\ 0 & 0 & -\nabla^2 \end{pmatrix}, \quad (41a)$$

$$H_{SOC} = -\sqrt{2}i \begin{pmatrix} \sqrt{2}\gamma_z\partial_z & \gamma_x\partial_x - i\gamma_y\partial_y & 0 \\ \gamma_x\partial_x + i\gamma_y\partial_y & 0 & \gamma_x\partial_x - i\gamma_y\partial_y \\ 0 & \gamma_x\partial_x + i\gamma_y\partial_y & -\sqrt{2}\gamma_z\partial_z \end{pmatrix} \quad (41b)$$

Since H_{SOC} can be considered to be consisting of sum of two commuting Hamiltonians, i.e.,

$$\begin{aligned} H_{SOC} &= -\sqrt{2}i \left[\begin{pmatrix} 0 & \gamma_x\partial_x - i\gamma_y\partial_y & 0 \\ \gamma_x\partial_x + i\gamma_y\partial_y & 0 & \gamma_x\partial_x - i\gamma_y\partial_y \\ 0 & \gamma_x\partial_x + i\gamma_y\partial_y & 0 \end{pmatrix} + \sqrt{2}\gamma_z \begin{pmatrix} \partial_z & 0 & 0 \\ 0 & 0 & 0 \\ 0 & 0 & -\partial_z \end{pmatrix} \right], \\ &= H_{xy} + H_z. \end{aligned} \quad (42)$$

With this division of H_{SOC} in 3D case, H_{xy} becomes identical to H_{SOC} defined in Eq. (35b) for q2D case. The second Hamiltonian H_z being diagonal can be combined with H_{KE} . In other words, we can redefine H_{SOC} as simply H_{xy} and H_{KE} as follows

$$H_{\text{KE}} = \begin{pmatrix} -\nabla^2 - 2i\gamma_z\partial_z & 0 & 0 \\ 0 & -\nabla^2 & 0 \\ 0 & 0 & -\nabla^2 + 2i\gamma_z\partial_z \end{pmatrix}. \quad (43)$$

The advantage of this redefining H_{SOC} making it identical to H_{SOC} in q2D case is that solution to equation (25b) is again given by Eq. (39) in Fourier space, whereas solution to Eq. (25a) with H_{KE} defined in Eq. (43) is given by

$$\begin{aligned} \hat{\phi}_{\pm 1}(k_x, k_y, k_z, t + \delta t) &= \hat{\phi}_{\pm 1}(k_x, k_y, k_z, t) \exp[-i(k_x^2 + k_y^2 + k_z^2 \pm 2\gamma_z k_z)\delta t], \\ \hat{\phi}_0(k_x, k_y, k_z, t + \delta t) &= \hat{\phi}_0(k_x, k_y, k_z, t) \exp[-i(k_x^2 + k_y^2 + k_z^2)\delta t]. \end{aligned}$$

3.2. Discretization Scheme

In the current study, spin-1 BECs considered are either confined by external trapping potential or are self-localized by the interplay of the interactions and spin-orbit coupling. This suggests that we can truncate our system from infinite space to some finite domain. In order to solve any equation computationally, we need to discretize our variables. We start by first truncating the spatial domain of the condensate along $\eta = x, y, z$ direction to L_η . Now, we choose $L_\eta = N_\eta \times \Delta\eta$, where $\Delta\eta$ is the space-step size chosen to discretize the spatial variable $\eta \in [-L_\eta/2, L_\eta/2]$ by setting $\eta_p = -L_\eta/2 + (p-1)\Delta\eta$ with $p = 1, 2, \dots, N_\eta + 1$. The point $\eta_{N_\eta+1}$ is excluded from the set of the grid points due the periodicity of the wavefunction, $\phi(\eta_{N_\eta+1}, t_q) = \phi(\eta_1, t_q)$. Similarly, time is discretized using Δt as temporal step size. The discretization in the Fourier space which avoids the aliasing condition can be achieved by discretizing k_η in N_η equispaced k_η points $\in \left[\frac{-N_\eta\pi}{L_\eta}, \dots, \frac{(N_\eta-2)\pi}{L_\eta} \right]$ with a spacing of $2\pi/L_\eta$. The resultant discretized wavefunction $\phi_j(\eta_p, t_q)$ ($\hat{\phi}_j(k_\eta^p, t_q)$) in real (Fourier) space, where p is the spatial (Fourier frequency) index and q is the time index, make these amenable to be discrete Fourier transformed by FFTW software library (where ‘‘in forward Fourier transform, positive frequencies are stored in the first half of the output and the negative frequencies are stored in backwards order in the second half of the output’’) [43], if k_η^p are indexed as

$$k_\eta(i) = (i-1)\frac{2\pi}{L_\eta}, \quad i = 1, \dots, \frac{N_\eta}{2} + 1, \quad (44)$$

$$k_\eta(i + 1 + \frac{N_\eta}{2}) = -k_\eta(1 - i + \frac{N_\eta}{2}), \quad i = 1, \dots, \frac{N_\eta}{2} - 1. \quad (45)$$

To summarize, the discrete analogues of the various continuous variables are as follows:

$$\eta \equiv \eta_p, \quad k_\eta \equiv k_\eta^p, \quad t \equiv t_q, \quad (46)$$

$$\phi_j(\eta, t) \equiv \phi_j(\eta_p, t_q), \quad \hat{\phi}_j(k_\eta, t) \equiv \hat{\phi}_j(k_\eta^p, t_q). \quad (47)$$

The N_η is chosen to be the multiple of 2 to have the best performance from the FFTW subroutines [43].

3.3. Imaginary-time propagation

We use imaginary-time propagation, wherein δt is replaced by $-i\delta t$, to compute the ground state of spin-1 BEC. This method neither preserves the norm nor the magnetization \mathcal{M} . To simultaneously fix the norm and magnetization, the component wavefunctions are redefined as

$$\phi_j(x^p, t_q) \equiv \sigma_j \phi_j(x^p, t_q), \quad (48)$$

after each iteration in imaginary time where σ_j are three projection parameters defined as [24]

$$\sigma_0 = \frac{\sqrt{1 - \mathcal{M}^2}}{[N_0 + \sqrt{4(1 - \mathcal{M}^2)N_1N_{-1} + (\mathcal{M}N_0)^2}]^{1/2}}, \quad (49)$$

$$\sigma_1 = \sqrt{\frac{1 + \mathcal{M} - (\sigma_0)^2 N_0}{2N_1}}, \quad \sigma_{-1} = \sqrt{\frac{1 - \mathcal{M} - (\sigma_0)^2 N_0}{2N_{-1}}}. \quad (50)$$

This simultaneous fixing of norm and \mathcal{M} is not implemented in the presence of SO-coupling rather only the total norm is fixed. The reason being the existence of ground state solution with arbitrary magnetization is not guaranteed in this case.

4. Details about the programs

In this section, we describe the set of three codes written in FORTRAN 90 programming language. These three programs, namely **imretime_spin1_1D.f90**, **imretime_spin1_2D.f90**, and **imretime_spin1_3D.f90**, correspond to solving 1D Eqs. (18a)-(18c), 2D Eqs. (14a)-(14c) and 3D Eqs. (10a)-(10c), respectively, using the time-splitting spectral method described in the previous section. Each of these programs can solve the aforementioned equations with the user defined *option* of either imaginary-time or real-time propagation.

The basic structure of the three codes is same; thus allowing us to describe the parameters, variables, modules, functions and subroutines using 1D code as a prototypical example.

4.1. Modules

First we provide the description of the four modules: BASIC_DATA, CGPE_DATA, SOC_DATA, FFTW_DATA.

BASIC_DATA

The input parameters like the number of iterations (NITER), number of spatial-grid points (NX), spatial and temporal step sizes (DX and DT) are defined at the top of each program in this module. Besides these parameters, number of OpenMP/FFTW threads, constants like π (PI), $i = \sqrt{-1}$ (CI), atomic mass unit (AMU), \hbar (HBAR) and spatial domain L_x (LX) are also defined in this module.

CGPE_DATA

The FORTRAN variables corresponding to k_x (KX), x (X), $V(x)$ (V), a_{osc} (AOSC), ω_x (OMEGAM), c_0 (C0), c_2 (C2), \mathcal{M} (MAG), $\phi_j(x)$ (PHI), $\hat{\phi}_j(k_x)$ (PHIF) are declared in this module. The scattering lengths a_0 (A0), a_2 (A2); anisotropy parameters α_x (ALPHAX), α_y (ALPHAY), and α_z (ALPHAZ); mass m (M) and total number of atoms N (NATOMS) are defined in this module. In addition to this there are two user defined integer options: (a) SWITCH_IM which has to

be set equal to 1 for imaginary-time propagation or 0 for real-time propagation and (b) `OPTION_FERRO_POLAR` which has to be set equal to 1, 2 or 3. `OPTION_FERRO_POLAR = 1, 2` correspond to suitable initial guess wavefunction for ferromagnetic and antiferromagnetic systems, respectively; whereas `OPTION_FERRO_POLAR = 3` implies that the Gaussian initial guess wavefunctions would be used.

SOC_DATA

The strength of spin-orbit coupling γ_x (`GAMMAX`) is defined in this module. `SWITCH_SOC` defined in this module has to be set equal to 1 if $\gamma_x \neq 0$ or equal to 0 if $\gamma_x = 0$. **The parameters and variables not listed in aforementioned three modules are not needed to be modified by the user.**

FFTW_DATA

The variable types of the input and output arrays used in FFTW subroutine to calculate discrete Fourier transform, requisite plans, and thread initialization variable are declared in this module. The module uses the FFTW3 module from the FFTW software library [43], and is not required to be modified by the user.

4.2. Functions and subroutines

Now, we will describe the functions and subroutines which have been used in the programs.

SIMPSON: This function evaluates one-dimensional integral of form $\int f(x)dx$ using Simpson's 1/3 rule adapted for even number of grid points.

DIFF: This function evaluates $\partial f(x)/\partial x$ using nine point Richardson's extrapolation formula.

INITIALIZE: This subroutine initializes the initial guess wavefunctions PHI, space mesh X, trapping potential V, and Fourier frequencies KX.

NORMT: The subroutine normalizes the total density to 1.

NORMC: The subroutine calculates the norms of the individual components, i.e. $\int |\phi_j(x)|^2 dx$.

RAD: The subroutine calculates the root mean square (rms) sizes of the three components.

ENERGY: The subroutine calculates the component chemical potentials μ_j (MU), E (EN), and \mathcal{M} (MAG).

FFT: The subroutine calculates the discrete forward Fourier transform using freely available FFTW software library [43]. The subroutine uses the module FFTW3.

BFT: Similarly, the subroutine calculates the discrete backward Fourier transform using FFTW software library [43].

KE: The subroutine evaluates Eq. (27) in Fourier space.

SOC: The subroutine implements Eq. (30) with \hat{H}_{SOC} given by Eq. (29).

SE: The subroutine implements Eq. (32) for H_{SE} consisting of spin-exchange terms.

SP: The subroutine implements Eq. (34) for H_{SP} consisting of spin-preserving terms.

4.3. 2D and 3D programs

As compared to 1D program which has NX grid points with spacing of DX , the 2D program requires $NX \times NY$ grid points with uniform spacing of DX and DY along x and y directions. This translates into spatial domain along the two directions as $LX = DX \times NX$, $LY = DY \times NY$. Similarly, 3D program requires $NX \times NY \times NZ$ grid points with corresponding space steps of DX , DY and DZ . The spatial domain along three directions here is $LX = DX \times NX$, $LY = DY \times NY$, $LZ = DZ \times NZ$. The additional space variables Y and/or Z would also require corresponding Fourier frequencies KY and/or KZ in 2D and 3D codes. The role of various subroutines is the direct extension of the roles played by them in 1D code as per the discussion in sections 3.1.1 and 3.1.2.

4.4. Running the programs

One has to install FORTRAN compiler(s) and FFTW software library on the computer. If user is interested in finding the ground state of the spin-1 BEC, the imaginary-time propagation has to be used. The dynamics on the other hand can be studied by real-time propagation using initial wave function which needs to be supplied by the user in the file 'initial_sol.dat'. The compilation commands are listed at the top of each program file and also in the 'README.txt' file provided with the codes.

4.5. Description of Output files

Data is written in four files during and after the execution of the 1D or 2D programs is complete. In the imaginary-time propagation, total norm, rms sizes of the components, energy, absolute values of component wavefunctions at origin, and magnetization are written after every NSTP iterations, which is defined in the BASIC_DATA module, in the file "file1_im.dat". In file "file2_im.dat", energy, chemical potentials, and rms sizes corresponding to each component are written after every STP iterations which is equivalent 0.1 (dimensionless) time period. In the file "tmp_solution_file.dat", which is updated after each NSTP iterations, component densities ρ_j and corresponding phases are written at every space point. The final ρ_j and corresponding phases are written in "solution_file_im.dat". In real-time-propagation, the corresponding file names are 'file1_re.dat', 'file2_re.dat' and so on. There is another file, namely "convergence.dat" which is written only in imaginary-time propagation. In this file $\max |\phi_j(x_p, t_q) - \phi_j(x_p, t_q - \Delta t)| / (2\Delta t)$ where $-L_x/2 \leq x_p < L_x/2$, $i = -1, 0, 1$ and t_q is the discrete imaginary-time is written after each iteration. This quantity serves as suitable convergence parameter, and the execution of the program is stopped if it falls below a user defined tolerance (TOL) defined in the CGPE_DATA module. *For all the results presented in this work a convergence tolerance of 10^{-6} has been met.*

In 3D code, besides the aforementioned four files, reduced densities in $x - y$ and $x - z$ planes and the corresponding phases are written in the files "tmp_solution_file_xy.dat" and "tmp_solution_file_xz.dat", respectively.

4.6. Output samples from the codes

Here we present the details of sample output files ‘file1_im.dat’ and/or ‘file1_re.dat’ obtained from three codes. The contents of this file written in the successive filled lines are: (1) time stamp at the time of start; (2) number of OpenMP and FFTW threads used in the run; (3) values of SWITCH_IM, OPTION_FERROPOLAR, SWITCH_SOC, SO coupling strengths (GAMMAX, GAMMAY, GAMMAZ), and tolerance (TOL) used; (4) values of anisotropy parameters (ALPHAX, ALPHAY, ALPHAZ) chosen; (5) number of space grid points (NX, NY, NZ); (6) values of NITER and NSTP; (7) value of space step(s) (DX, DY, DZ), (7) time step DT, space domain (LX, LY, LZ), and magnetization (MAG); (8) frequency used in scaling (OMEGAM), corresponding oscillator length (AOSC), and values of interaction parameters (C0, C2). Then total norm, rms sizes of the component wavefunctions, energy, absolute values of component wavefunctions at the origin, and magnetization are written for initial solution, for the transient solution obtained after NSTP time iterations and for the converged solution (this third entry in real-time code will simply correspond to the solution after NITER iterations). The time stamp at the end of the run and execution time are the last two entries in this file. The varied nature of the contents of this file can be used to ascertain the success of the run of the code by verifying the input parameters selected and various output parameters. The sample output files obtained with the test runs of imretime_spin1_1D.f90, imretime_spin1_2D.f90, and imretime_spin1_3D.f90 are presented in the Electronic Appendix. In all the test runs, harmonic trapping potential as per the trapping potential corresponding to anisotropy parameters listed in these files have been used. For these test runs, the codes were compiled with Intel’s FORTRAN compiler and the jobs were run on a server with two Intel® Xeon® Platinum 8180 CPU @ 2.50GHz. The samples of all the data files, both input and output, corresponding to the current set of parameters in the codes are available on Mendeley data [44].

5. OpenMP Parallelization

We have tested the efficiency of OpenMP parallelization of the three codes for both imaginary and real-time propagations. The tests were done on a 28-core Intel® Xeon® Platinum 8180 CPU @ 2.50GHz processor. The parallelization tests were performed with $NX = 10^6$ for 1D code, $NX = NY = 3000$ for 2D code, and $NX = NY = 256, NZ = 128$ for 3D code. The execution time was measured for 1000 iterations starting from the call to INITIALIZE subroutine and did not include the time spent in reading/writing and opening/closing the data files. The execution times $T(n)$ for the three codes compiled with both GNU Fortran 5.4.0 and Intel Fortran 19.1.0.166 compilers are shown as a function of number of threads n in Fig. 1. It is evident from Fig. 1 that the codes compiled with Intel Fortran compiler are faster than those compiled with GNU Fortran compiler for both the imaginary time and real-time propagations; nonetheless the difference in the execution times for codes compiled with these two compilers is less for real-time propagation. The execution times in all the cases shown in Fig. 1 first decrease very sharply with the increase in the number of threads and then tends to saturate with increasing number of threads.

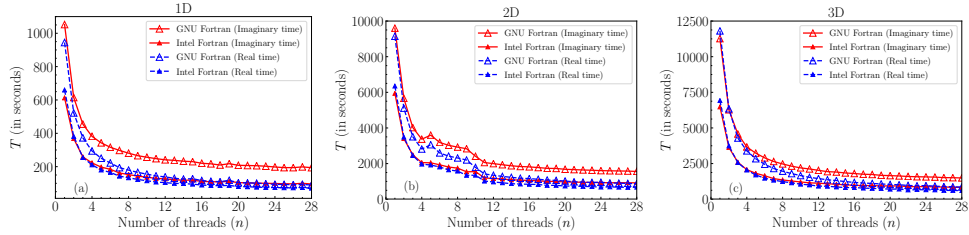


Figure 1: (Color online) (a) Execution times for 1000 iterations (in seconds) as function of number of threads for 1D code compiled with GNU Fortran 5.4.0 and Intel Fortran 19.1.0.166 compilers for imaginary and real-time propagation. (b) and (c) are the same for 2D and 3D codes.

To quantify the performance gain with OpenMP parallelization, we have calculated the speedup and efficiency for all these codes compiled with the aforementioned two compilers. Here speedup is defined as the ratio of execution time with 1 thread to the execution time with n threads, i.e. $T(1)/T(n)$, whereas the efficiency is defined as the ratio $T(1)/[nT(n)]$. For all the codes, speedup and efficiency as a function of number of threads are much better for real-time propagation as compared to imaginary time propagation. The real-time speedup achieved with 28 threads was more than 9 for both 1D and 2D codes, and more than 11 for 3D code using both the compilers; whereas the corresponding imaginary time speedup values are more than 5 for 1D, more than 6 for 2D and more than 7 for 3D with both the compilers as is shown in Fig. 2. The best performing real-time 3D has more than 40% efficiency with 28 threads. The better performance of real-time variants is due to fact that the imaginary propagation has to fix the norm and also has to check the convergence criterion during each iteration. Real-time propagation corresponds to the unitary evolution of a converged solution, and hence does not need to fix the norm or check the convergence. All the results presented in this section were performed for non-zero value of SO-coupling strength.

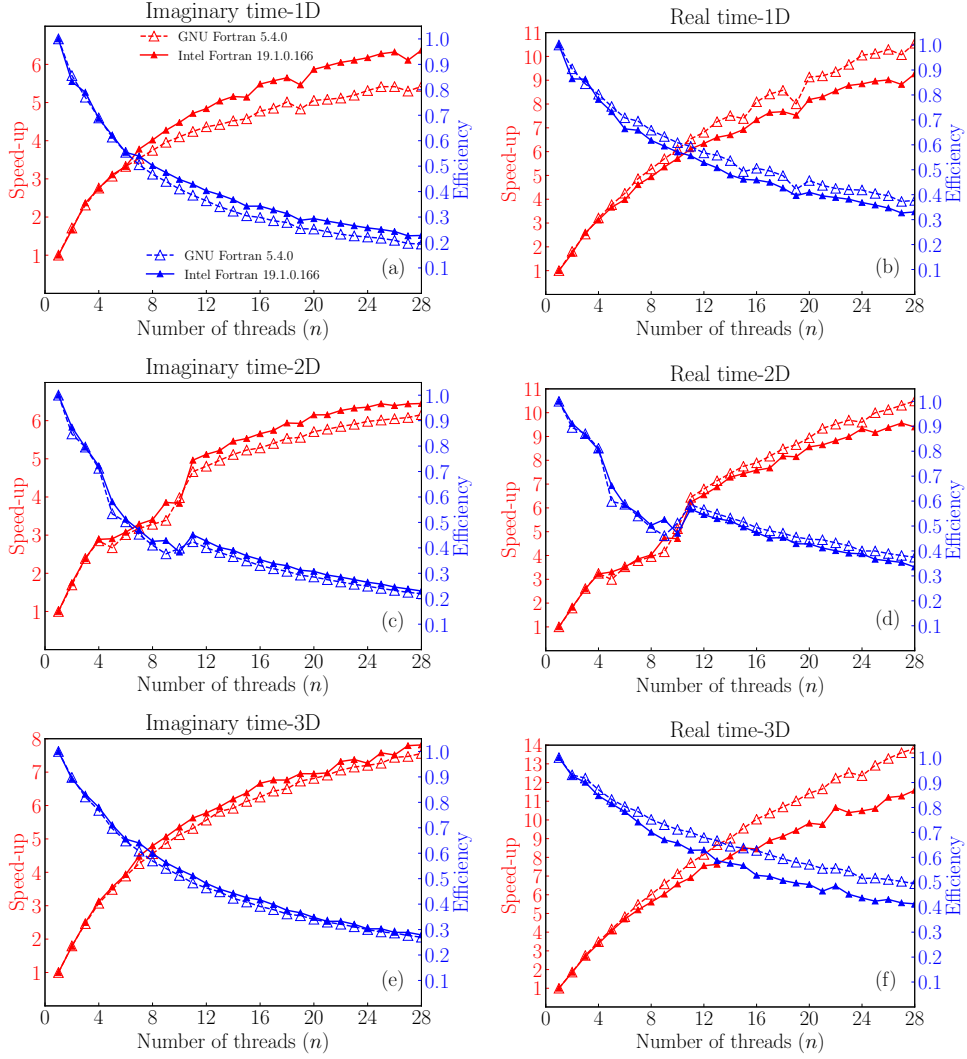


Figure 2: (Color online) Speedup and efficiency as a function of number of threads n are shown for imaginary time (left column) and real-time propagation (right column). Top, middle and bottom row figures show the results for 1D, 2D and 3D codes, respectively.

6. Numerical Results

In this section, we present the results for energy, chemical potentials, and densities of the ground states in q1D, q2D and 3D spin-1 condensates using the imaginary time propagation method with the emphasis on the comparison with the previously published results in the literature [24, 25, 38, 40, 41]. We report the results in the presence as well as absence of SO coupling.

To check the accuracy of numerical method employed by us, we compare our results in the absence of SO coupling with those in Ref. [24, 25]. In the presence of SO coupling, we compare our results in q1D, q2D and 3D spin-1 BECs with those in Refs. [38], [40] and [41] respectively. It needs to emphasized that the method used in Ref. [25] is not applicable to SO-coupled spin-1 BECs.

6.1. Results for q1D spin-1 BECs

6.1.1. Without SO coupling, $\gamma_x = 0$

We choose our computational domain $L = [-16, 16]$ having spatial step size as $\Delta x = 1/64$ for q1D condensates. We first consider (a) ferromagnetic spin-1 BEC of ^{87}Rb confined in a cigar-shaped trapping potential having interaction parameters in dimensionless units as $c_0 = 0.0885N$ and $c_2 = -0.00041N$ [24] and (b) antiferromagnetic spin-1 condensate of ^{23}Na confined in a cigar-shaped trapping potential having interaction parameters in dimensionless units as $c_0 = 0.0241N$ and $c_2 = 0.00075N$ [24, 25] for our computations in one dimensional case. We consider $N = 10^4$ as the total number of atoms in each of these two cases. The comparison of ground state energies obtained in present work with those in Refs. [24, 25] is excellent as is shown in table 1 for $\Delta x \leq 1/64$ and $\Delta t \approx 0.1\Delta x^2$

Table 1: Ground state energies for ^{87}Rb and ^{23}Na q1D BECs obtained in the present work with $\Delta x \leq 0.015625$ and $\Delta t \approx 0.1\Delta x^2$ along with the same from Ref [24] for the various values of magnetization \mathcal{M} .

\mathcal{M}	^{87}Rb		^{23}Na	
	E in Ref.[24]	E (present work)	E in Ref. [24, 25]	E (present work)
0	36.1365	36.1365	15.2485	15.2485
0.1	36.1365	36.1365	15.2513	15.2513
0.2	36.1365	36.1365	15.2599	15.2599
0.3	36.1365	36.1365	15.2743	15.2743
0.4	36.1365	36.1365	15.2945	15.2945
0.5	36.1365	36.1365	15.3209	15.3209
0.6	36.1365	36.1365	15.3537	15.3537
0.7	36.1365	36.1365	15.3933	15.3933
0.8	36.1365	36.1365	15.4405	15.4405
0.9	36.1365	36.1365	15.4962	15.4962

For q1D ^{87}Rb , we also consider an alternative set of interaction parameters of $c_0 = 0.08716N$, $c_2 = -0.001748N$ and $N = 10000$ for our computations [25]. In this case again, the ground state energy obtained in the present work is in excellent agreement with the value reported in Ref. [25] as is shown in table 2 for the same interaction parameters set.

Table 2: Comparison of the ground state energy of q1D ^{87}Rb condensate reported in Ref. [25] with the value obtained in the present work with $\Delta x \leq 0.0156255$ and $\Delta t \approx 0.1\Delta x^2$

	^{87}Rb	
\mathcal{M}	E in Ref. [25]	E (present work)
0-0.9	35.4007	35.4007[7]

The chemical potential values obtained in present work are also in very good agreement with those reported in Ref. [24] as is shown in table 3.

Table 3: Comparison of the chemical potential values for ^{87}Rb and ^{23}Na condensate reported in Ref. [24] with the values obtained in the present work with $\Delta x = 0.0025$, $\Delta t = 0.0000095$. For ^{23}Na , $\mu = (\mu_{+1} + \mu_{-1})/2$, whereas for ^{87}Rb $\mu = \mu_0 = \mu_{\pm 1}$.

	^{87}Rb		^{23}Na	
\mathcal{M}	μ in Ref. [24]	μ (present work)	μ in [24]	μ (present work)
0	60.2139	60.2136	25.3857	25.3857
0.1	60.2139	60.2136	25.3847	25.3838
0.2	60.2139	60.2136	25.3815	25.3804
0.3	60.2139	60.2136	25.3762	25.3749
0.4	60.2139	60.2137	25.3682	25.3668
0.5	60.2139	60.2137	25.3572	25.3557
0.6	60.2139	60.2137	25.3423	25.3406
0.7	60.2139	60.2138	25.3220	25.3203
0.8	60.2139	60.2138	25.2939	25.2921
0.9	60.2139	60.2139	25.2527	25.2509

The ground state wavefunctions are also in excellent agreement with Ref. [24]. The absolute values of ground state wavefunctions for ^{87}Rb and ^{23}Na with $\mathcal{M} = 0$ and 0.5 are shown in Fig. 3.

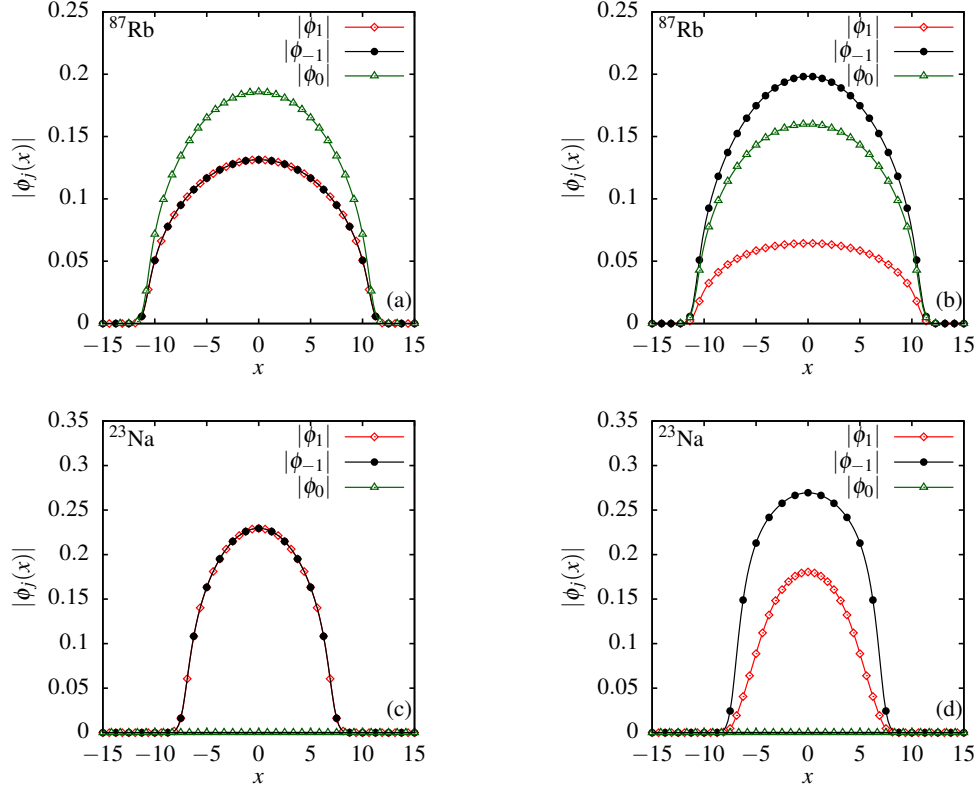


Figure 3: (Color online) Absolute values of component wavefunctions $|\phi_j(x)|$ in the ground state of ^{87}Rb for (a) $M = 0$, (b) $M = 0.5$. (c) and (d) are the same for ^{23}Na with $M = 0$ and $M = 0.5$, respectively. These are in agreement with [24, 25]

6.1.2. With SO coupling, $\gamma_x \neq 0$

In the presence of SO coupling with harmonic trapping potential, for ^{87}Rb and ^{23}Na , we again consider (c_0, c_2) equal to $(0.08716N, -0.001748N)$ and $(0.0241N, 0.00075N)$, respectively, where $N = 10000$. The ground state energy values in these cases are given in table 4 for multiple values of γ_x . The component densities for the two systems with $\gamma_x = 0.5$ and 1 are shown in Fig. 4.

Table 4: Ground state energies of ^{87}Rb and ^{23}Na condensates in the presence of harmonic trap and spin-orbit coupling with $\Delta x = 0.015625$, $\Delta t \approx 0.1(\Delta x)^2$. The (c_0, c_2) values are $(0.08716N, -0.001748N)$ and $(0.0241N, 0.00075N)$ with $N = 10000$ for ^{87}Rb and ^{23}Na , respectively.

	^{87}Rb	^{23}Na
γ_x	Energy	Energy
0	35.4007	15.2485
0.1	35.3958	15.2435
0.2	35.3808	15.2285
0.3	35.3558	15.2035
0.4	35.3208	15.1685
0.5	35.2758	15.1235
0.6	35.2208	15.0685
0.7	35.1558	15.0035
0.8	35.0808	14.9285
0.9	34.9958	14.8435
1	34.9008	14.7485

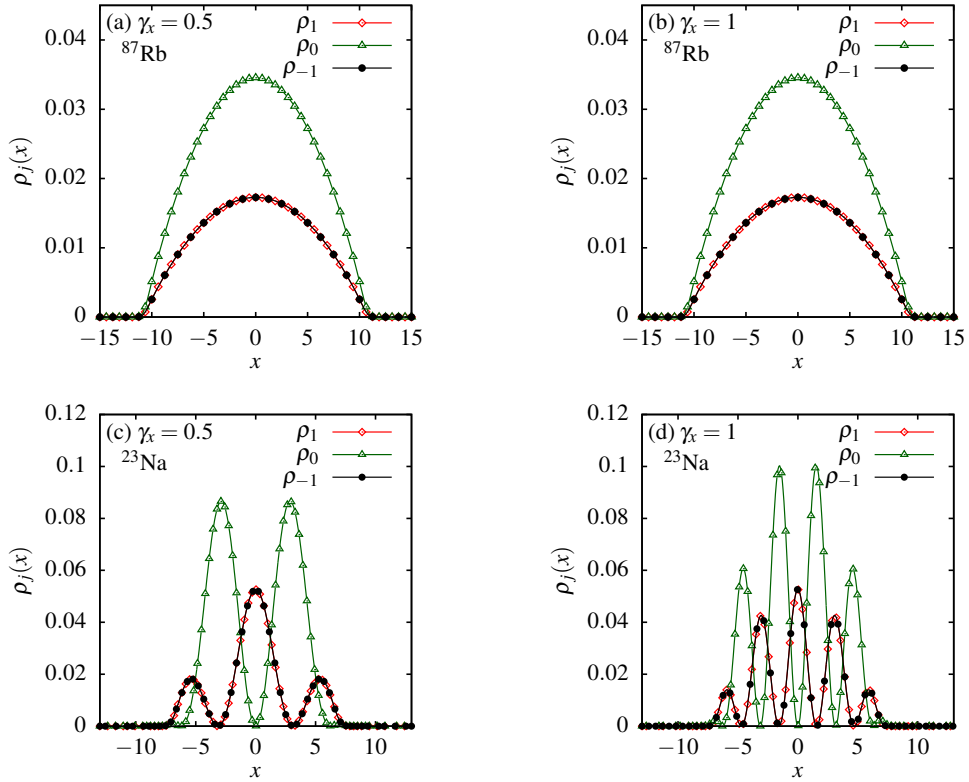


Figure 4: (Color online) Ground state density of SO-coupled ^{87}Rb for (a) $\gamma_x = 0.5$, (b) $\gamma_x = 1$. (c) and (d) are the same for ^{23}Na with $\gamma_x = 0.5$ and $\gamma_x = 1.0$, respectively. $M = 0$ in all the cases.

Next, we consider ferromagnetic and antiferromagnetic systems with (c_0, c_2) equal to $(-1.5, -0.3)$ and $(-1.2, 0.3)$, respectively in the absence of any trapping. The ground state energies of the self-trapped solutions obtained in these cases are shown in table 5. The self-trapped nature of the

Table 5: Ground state energies for self-trapped ferromagnetic and antiferromagnetic condensates in the presence of spin-orbit coupling obtained with $\Delta x = 0.015625$, $\Delta t \approx 0.1(\Delta x)^2$.

	$(c_0, c_2) = (-1.5, -0.3)$	$(c_0, c_2) = (-1.2, 0.3)$
γ_x	Energy	Energy
0	-0.1350	-0.0600
0.1	-0.1400	-0.0650
0.2	-0.1550	-0.0800
0.3	-0.1800	-0.1050
0.4	-0.2150	-0.1400
0.5	-0.2600	-0.1850
0.6	-0.3150	-0.2400
0.7	-0.3800	-0.3050
0.8	-0.4550	-0.3800
0.9	-0.5400	-0.4650
1	-0.6350	-0.5600

solutions is evident from the ground state densities shown in Fig. 5 for $\gamma_x = 1$.

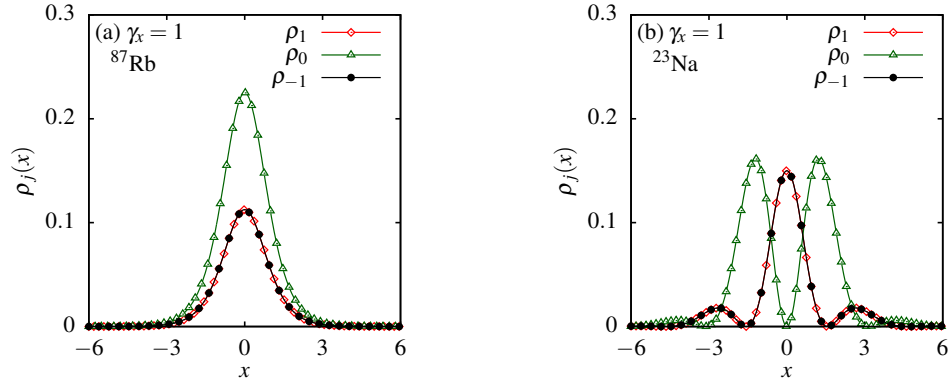


Figure 5: (Color online) (a) Ground state density of SO-coupled spin-1 BEC with $c_0 = -1.5$, $c_2 = -0.3$ in the absence of trap and $\gamma_x = 1$. (b) The same for $c_0 = -1.2$, $c_2 = 0.3$. These results are in agreement with Ref. [41] and correspond to $M = 0$.

6.2. Real-time check

To check the stationary nature of the solutions one can evolve these solutions using real-time propagation. As an example, we consider the real-time evolution of a self-trapped solution of

q1D ^{87}Rb condensate with $c_0 = -1.5, c_2 = -0.3$ and $\gamma_x = 0.5$, which has $E = -0.2600$ as indicated in table 5. The rms size of the three components of the vector soliton as a function of time is shown in Fig. 6(a). Similarly, energy E as a function of t is shown in Fig. 6(b) which agrees with reported value of -0.2600 at all the times. All the results reported in this work confirm with this real-time evolution check.

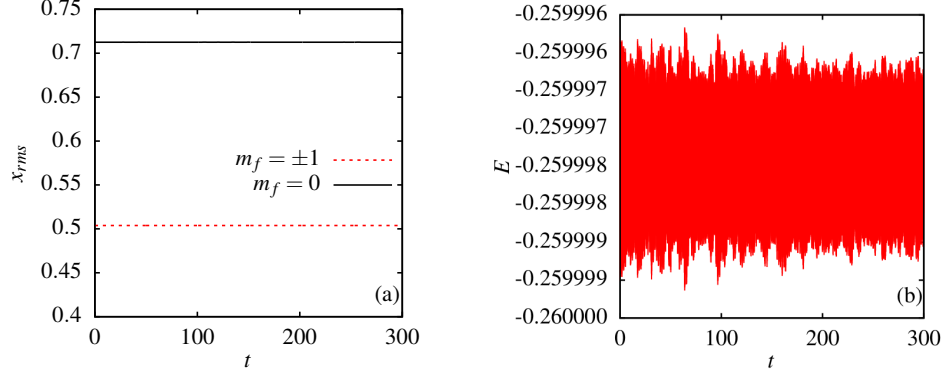


Figure 6: (Color online) (a) Root mean square sizes of the three components of ^{87}Rb with $c_0 = -1.5, c_2 = -0.3$ and $\gamma_x = 0.5$ in the absence of trap as a function of time. (b) Energy of the vector soliton as function of time.

6.3. Results for q2D and 3D spin-1 BECs

Here we first consider 10^4 atoms of ^{87}Rb with $(a_0, a_2) = (5.387, 5.313)$ nm in a q2D trap with $\alpha_x = \alpha_y = 1, \alpha_z = 20, \omega_x/(2\pi) = 20\text{Hz}$. Secondly, we consider 10^4 atoms of ^{23}Na with $(a_0, a_2) = (2.646, 2.911)$ nm in a q2D trap with same trapping frequencies as that for ^{87}Rb . This leads to $(c_0, c_2) = (496.4428, -2.2942)$ and $(134.9838, 4.2242)$ for ^{87}Rb and ^{23}Na , respectively. The ground state energies (in the units $\hbar\omega_x$) for various magnetizations are given in table 6.

Table 6: Ground state energies for ^{87}Rb and ^{23}Na q2D BECs obtained in the present work with $\Delta x = 0.05$, $\Delta y = 0.05$ and $\Delta t = 0.1\Delta x\Delta y/2$ for the various values of magnetization \mathcal{M} . 10^4 atoms of each species were considered in trap with $\alpha_x = \alpha_y = 1$, $\alpha_z = 20$, $\omega_x/(2\pi) = 20\text{Hz}$. Together with scattering lengths (a_0, a_2), these parameters define c_0 and c_2 as per Eq. (16).

	^{87}Rb	^{23}Na
\mathcal{M}	Energy	Energy
0	8.4629	4.5355
0.1	8.4629	4.5361
0.2	8.4629	4.5380
0.3	8.4629	4.5412
0.4	8.4629	4.5457
0.5	8.4629	4.5515
0.6	8.4629	4.5586
0.7	8.4629	4.5671
0.8	8.4629	4.5771
0.9	8.4629	4.5885

For q2D case, we also consider $c_0 = -4, c_1 = -0.6$ with $\gamma_x = \gamma_y = 0.5$, i.e isotropic SO coupling, in the absence of trapping. The ground state in this case is a self-trapped vortex-bright soliton as is shown in Fig. 7. The ground state solution corresponds to an asymmetric antivortex and vortex in the $m_f = +1$ and $m_f = -1$ components, respectively as is illustrated in Fig. 7(d)-(f) [40].

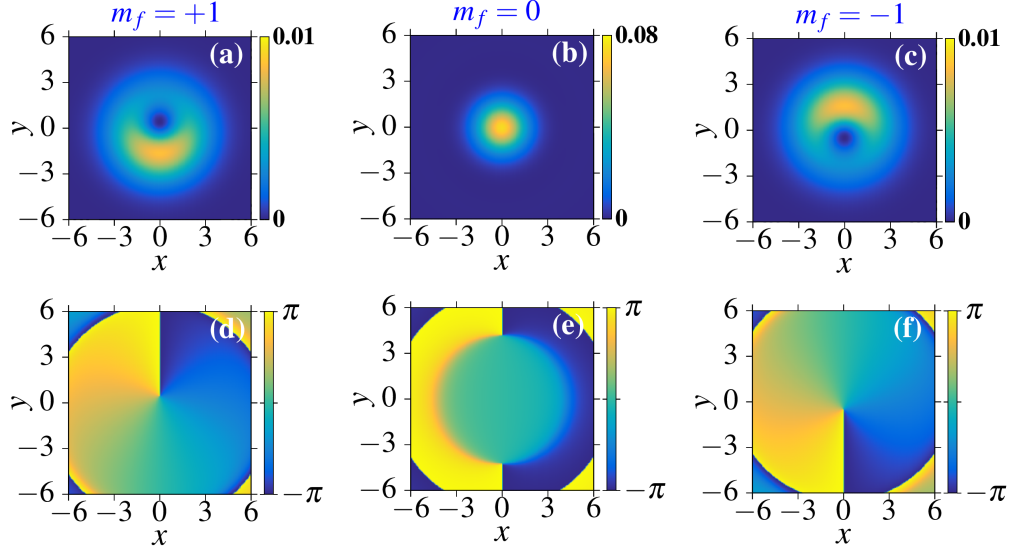


Figure 7: The 2D contour plot of densities of (a) $m_f = +1$, (b) $m_f = 0$, and (c) $m_f = -1$ components of an asymmetric vortex-bright soliton with $c_0 = -4$, $c_1 = -0.6$ and $\gamma_x = \gamma_y = 0.5$. The corresponding phases are shown in (d) for $m_f = +1$, (e) for $m_f = 0$ and (f) for $m_f = -1$ components.

Similarly in the 3D case, we consider $c_0 = -10$, $c_1 = 0.1$ with $\gamma_x = \gamma_y = \gamma_z = 1$ in the absence of trapping. Again, the ground state solution in this case is a self-trapped vortex-bright soliton. To illustrate this vortex-bright soliton, we plot the two-dimensional contour densities and corresponding phase profiles in $z = 0$ plane in Fig. 8. These results are in agreement with [38].

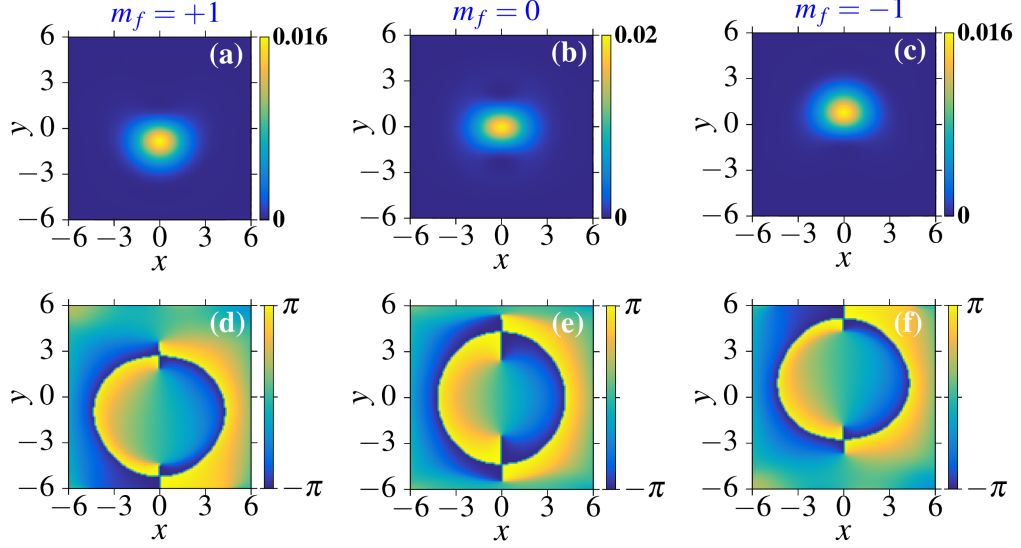


Figure 8: The 2D contour plots of densities of components in $z = 0$ plane for (a) $m_f = +1$, (b) $m_f = 0$, and (c) $m_f = -1$ of an asymmetric vortex-bright soliton with $c_0 = -10$, $c_1 = -1$ and $\gamma_x = \gamma_y = \gamma_z = 1$. The corresponding phases are shown in (d) for $m_f = +1$, (e) for $m_f = 0$, and (f) for $m_f = -1$ components.

7. Summary

We have discussed a time-splitting Fourier spectral method to solve the mean-field model of spin-1 BECs with anisotropic spin-orbit coupling. The time-splitting coupled with spectral method allows one to deal with non-linear and SO coupling terms very precisely. The numerical scheme has been implemented via three FORTRAN 90/95 codes, which are OpenMP parallelized, for quasi-one, quasi-two and three-dimensional spin-1 BECs. We have provided the results for execution time, speedup, and efficiency as a function of number of threads for the three codes. The numerical results obtained with the three codes are in very good agreement with previous results without SO coupling from the literature. The model of SO coupling is quite general enough to allow the users of the codes to simulate a variety of SO couplings considered in the literature which include Rashba SO coupling (isotropic or anisotropic), Dresselhaus SO coupling (isotropic or anisotropic) or their mixture. With the recent spur in the studies on SO coupled spinor BECs, the present numerical scheme along with the codes could be quite useful to the researchers exploring this field. The spectral method used in manuscript can be extended to solve the Stochastic projected coupled Gross-Pitaevskii equations for spin-1 BECs on one hand (here the implementation of the projection is quite natural in Fourier space) or simulate rotating Spin-1 BECs with or without SO coupling. These two directions may be explored in future projects.

Acknowledgments

AR acknowledges support from Provincia Autonoma di Trento. SG thanks the Science & Engineering Research Board, Department of Science and Technology, Government of India (Project: ECR/2017/001436) and Indian Institute of Technology, Ropar (ISIRD Project: 9-256/2016/IITRPR/823) for support. SG acknowledges the useful discussions with Prof. S. K. Adhikari of Instituto de Física Teórica, Universidade Estadual Paulista, São Paulo.

References

- [1] M.H. Anderson, J.R. Ensher, M.R. Matthews, C.E. Wieman, and E.A. Cornell, *Science* 269 (1995) 198; K.B. Davis, M.-O. Mewes, M.R. Andrews, N.J. van Druten, D.S. Durfee, D.M. Kurn, and W. Ketterle, *Phys. Rev. Lett.* 75 (1995) 3969; C.C. Bradley, C.A. Sackett, J.J. Tollett, and R.G. Hulet, *Phys. Rev. Lett.* 75 (1995) 1687.
- [2] D.M. Stamper-Kurn, M.R. Andrews, A.P. Chikkatur, S. Inouye, H.-J. Miesner, J. Stenger, and W. Ketterle, *Phys. Rev. Lett.* 80 (1998) 2027.
- [3] J. Stenger, S. Inouye, D.M. Stamper-Kurn, H.-J. Miesner, A.P. Chikkatur, and W. Ketterle, *Nature* 396 (1998) 345; M. D. Barrett, J. A. Sauer, and M. S. Chapman, *Phys. Rev. Lett.* 87 (2001) 010404. A.T. Black, E. Gomez, L.D. Turner, S. Jung, and P.D. Lett, *Phys. Rev. Lett.* 99 (2007) 070403; M.-S. Chang, C.D. Hamley, M.D. Barrett, J.A. Sauer, K.M. Fortier, W. Zhang, L. You, and M.S. Chapman, *Phys. Rev. Lett.* 92 (2004) 140403; A. Görlitz, T.L. Gustavson, A.E. Leanhardt, R. Löw, A.P. Chikkatur, S. Gupta, S. Inouye, D.E. Pritchard, and W. Ketterle, *Phys. Rev. Lett.* 90 (2003) 090401; H. Schmaljohann, M. Erhard, J. Kronjäger, M. Kottke, S. van Staa, L. Cacciapuoti, J.J. Arlt, K. Bongs, and K. Sengstock, *Phys. Rev. Lett.* 92 (2004) 040402; T. Kuwamoto, K. Araki, T. Eno, and T. Hirano, *Phys. Review A* 69 (2004) 063604; B. Pasquiou, E. Maréchal, G. Bismut, P. Pedri, L. Vernac, O. Gorceix, and B. Laburthe-Tolra, *Phys. Rev. Lett.* 106 (2011) 255303; D.M. Stamper-Kurn and M. Ueda, *Rev. Mod. Phys.* 85 (2013) 1191.
- [4] K. Osterloh, M. Baig, L. Santos, P. Zoller, and M. Lewenstein, *Phys. Rev. Lett.* 95 (2005) 010403; J. Ruseckas, G. Juzeliūnas, P. Öhberg, and M. Fleischhauer, *Phys. Rev. Lett.* 95 (2005) 010404; J. Dalibard, F. Gerbier, G. Juzeliūnas, and P. Öhberg, *Rev. Mod. Phys.* 83 (2011) 1523; N. Goldman, G. Juzeliūnas, P. Öhberg, and I.B. Spielman, *Rep. Prog. Phys.* 77 (2014) 126401.
- [5] Y.-J. Lin, K. Jiménez-García, and I.B. Spielman, *Nature* 471 (2011) 83.
- [6] Y.A. Bychkov and E.I. Rashba, *J. Phys. C: Solid state physics* 17 (1984) 6039.
- [7] G. Dresselhaus, *Phys. Rev.* 100 (1955) 580.
- [8] M. Aidelsburger, M. Atala, S. Nascimbéne, S. Trotzky, Y.-A. Chen, and I. Bloch, *Phys. Rev. Lett.* 107 (2011) 255301; Z. Fu, P. Wang, S. Chai, L. Huang, and J. Zhang, *Phys. Rev. A* 84 (2011) 043609; J.-Y. Zhang, S.-C. Ji, Z. Chen, L. Zhang, Z.-D. Du, B. Yan, G.-S. Pan, B. Zhao, Y.-J. Deng, H. Zhai, S. Chen, and J.-W. Pan, *Phys. Rev. Lett.* 109 (2012) 115301; C. Qu, C. Hamner, M. Gong, C. Zhang, and P. Engels, *Phys. Rev. A* 88 (2013) 021604.
- [9] C. Wang, C. Gao, C.-M. Jian, and H. Zhai, *Phys. Rev. Lett.* 105 (2010) 160403.
- [10] H. Zhai, *Int. J. Mod. Phys. B* 26 (2012) 1230001.
- [11] S. Sinha, R. Nath, and L. Santos, *Phys. Rev. Lett.* 107 (2011) 270401; H. Hu, B. Ramachandran, H. Pu, and X.-J. Liu, *Phys. Rev. Lett.* 108 (2012) 010402; Y. Xu, Y. Zhang, and B. Wu, *Phys. Review A* 87 (2013) 013614; L. Salasnich and B. A. Malomed, *Phys. Review A* 87 (2013) 063625; Salasnich, L., Cardoso, W. B., and Malomed, B. A., *Phys. Rev. A* 90 (2014) 033629; S. Cao, C.-J. Shan, D.-W. Zhang, X. Qin, and J. Xu, *JOSA B* 32 (2015) 201; H. Sakaguchi, B. Li, and B.A. Malomed, *Phys. Rev. E* 89 (2014) 032920; H. Sakaguchi and B.A. Malomed, *Phys. Rev. E* 90 (2014) 062922; Y.-K. Liu and S.-J. Yang, *Euro Phys. Lett.* 108 (2014) 30004; T.-L. Ho and S. Zhang, *Phys. Rev. Lett.* 107 (2011) 150403; Z.-F. Xu, L. You, and M. Ueda, *Phys. Rev. A* 87 (2013) 063634
- [12] V. Galitski and I.B. Spielman, *Nature* 494 (2013) 49.
- [13] C.L. Kane and E.J. Mele, *Phys. Rev. Lett.* 95 (2005) 146802; B.A. Bernevig, T.L. Hughes, and S.C. Zhang, *Science* 314 (2006) 1757; D. Hsieh, D. Qian, L. Wray, Y. Xia, Y. S. Hor, R.J. Cava, and M.Z. Hasan, *Nature* 452 (2008) 970; M.Z. Hasan, and C.L. Kane, *Rev. Mod. Phys.* 82 (2010) 3045; X.L. Qi and S.-C. Zhang, *Rev. Mod. Phys.* 83 (2011) 1057.
- [14] J.D. Koralek, C.P. Weber, J. Orenstein, B.A. Bernevig, S.-C. Zhang, S. Mack, and D.D. Awschalom *Nature* 458 (2009) 610.
- [15] A. Avsar *et al.*, *Nature Comm.* 5 (2014) 4875; Z. Wang, C. Tang, R. Sachs, Y. Barlas, and J. Shi, *Phys. Rev. Lett.* 114 (2015) 016603.
- [16] J.D. Sau, R.M. Lutchyn, S. Tewari, and S.D. Sarma, *Phys. Rev. Lett.* 104 (2010) 040502.
- [17] D.L. Campbell, R.M. Price, A. Putra, A. Valdés-Curiel, D. Trypogeorgos and I.B. Spielman, *Nature communications* 7 (2016) 10897.

- [18] Y.-K. Liu, G.-H. Yang, L.-L. Xu, and S.-J. Yang, *Ann. Phys.* 405 (2019) 289; L. Zhang, Y. Ke, and C. Lee, *Phys. Rev. B* 100 (2019) 224420; Y.V. Kartashov V.V. and Konotop, *Phys. Rev. Lett.* 118 (2017) 190401.
- [19] J.-R. Li, J. Lee, W. Huang, S. Burchesky, B. Shteynas, F.C. Top, A.O. Jamison, and W. Ketterle, *Nature* 543 (2017) 91; J. Li, W. Huang, B. Shteynas, S. Burchesky, F.C. Top, E. Su, J. Lee, A.O. Jamison, and W. Ketterle *Phys. Rev. Lett.* 117 (2016) 185301; S. Zhang, and G.-B. Jo, *Journal of Physics and Chemistry of Solids* 128 (2018) 75.
- [20] Zwartsenberg, B. *et al.*, *Nature Physics*, <https://doi.org/10.1038/s41567-019-0750-y>
- [21] T.-L. Ho, *Phys. Rev. Lett.* 81 (1998) 742.
- [22] T. Ohmi and K. Machida, *Journal of the Physical Society of Japan* 67 (1998) 1822.
- [23] H. Wang, *Int. J. Comp. Math.* 84 (2007) 925.
- [24] W. Bao and F.Y. Lim, F. Y., *SIAM Journal on Scientific Computing* 30 (2008) 1925.
- [25] W. Bao, I.-L. Chern, and Y. Zhang, *J. Comp. Phys.* 253 (2013) 189.
- [26] P. Ruprecht, M. Holland, K. Burnett, and M. Edwards, *Phys. Rev. A* 51 (1995) 4704; M. Edwards and K. Burnett, *Phys. Rev. A* 51 (1995) 1382. R. Dodd, *Journal of Research of the National Institute of Standards and Technology* 101 (1996) 545; W. Bao and W. Tang, *J. Comp. Phys.* 187 (2003) 230; W. Bao and Y. Cai, *SIAM Journal on Numerical Analysis* 50 (2012) 492; R.P. Tiwari and A. Shukla, *Comp. Phys. Comm.* 174 (2006) 966; W. Bao, W. and Y. Cai, *Mathematics of Computation* 82 (2013) 99.
- [27] M.L. Chiofalo, S. Succi, and M. Tosi, *Phys. Rev. E* 62 (2000) 7438
- [28] W. Bao and Q. Du, *SIAM Journal on Scientific Computing* 25 (2004) 1674
- [29] X. Antoine, W. Bao, and C. Besse, *Comp. Phys. Comm.* 184 (2013) 2621.
- [30] P. Muruganandam and S.K. Adhikari, *Comp. Phys. Comm.* 180 (2009) 1888
- [31] W. Bao, D. Jaksch, and P.A. Markowich, *J. Comp. Phys.* 187 (2003) 318.
- [32] S.-M. Chang, W.-W. Lin, and S.-F. Shieh, *J. Comp. Phys.* 202 (2005) 367; W. Bao and J. Shen, *SIAM Journal on Scientific Computing* 26 (2005) 2010.
- [33] H. Wang and Z. Xu, *Comp. Phys. Comm.* 185 (2014) 2803; H. Wang, *J. Comp. Phys.* 274 (2014) 473.
- [34] W. Bao, S. Jin, P.A. Markowich, *J. Comp. Phys.* 175 (2002) 487; W. Bao, S. Jin, P.A. Markowich, *SIAM Journal on Scientific Computing*, 25 (2003) 27.
- [35] L.E. Young-S., P. Muruganandam, S.K. Adhikari, V. Loncar, D. Vudragovic, A. Balaz *Comput. Phys. Commun.* 220 (2017) 503; V. Loncar, L.E. Young-S., S. Skrbic, P. Muruganandam, S.K. Adhikari, *Antun Balaz Comput. Phys. Commun.* 209 (2016) 190; L.E. Young-S., D. Vudragovic, P. Muruganandam, S.K. Adhikari, A. Balaz *Comput. Phys. Commun.* 204 (2016) 209; B. Sataric, V. Slavnic, A. Belic, A. Balaz, P. Muruganandam, S.K. Adhikari *Comput. Phys. Commun.* 200 (2016) 411; V. Loncar, A. Balaz, A. Bogojevic, S. Skrbic, P. Muruganandam, S.K. Adhikari *Comput. Phys. Commun.* 200 (2016) 406; D. Vudragovic, I. Vidanovic, A. Balaz, P. Muruganandam, S.K. Adhikari *Comput. Phys. Commun.* 183 (2012) 2021; X. Antoine and R. Duboscq *Comput. Phys. Commun.* 185 (2014) 2969; X. Antoine and R. Duboscq *Comput. Phys. Commun.* 193 (2015) 95; Ž. Marojević and E. Göklü and Claus Lämmerzahl *Comput. Phys. Commun.* 202 (2016) 216
- [36] J.L. Ville R. Saint-Jalm, É. Le Cerf, M. Aidelsburger, S. Nascimbène, J. Dalibard, and J. Beugnon, *Phys. Rev. Lett.* 121 (2018) 145301.
- [37] D.L. Campbell and I.B. Spielman, *New Journal of Physics* 18 (2016) 033035.
- [38] S. Gautam, and S.K. Adhikari, *Phys. Rev. A* 97 (2018) 013629.
- [39] L. Salasnich, A. Parola, and L. Reatto, *Phys. Rev. A* 65 (2002) 043614; L. Salasnich, A. Parola, and L. Reatto, *Phys. Rev. A* 72 (2005) 025602.
- [40] S. Gautam and S.K. Adhikari, *Phys. Rev. A* 95 (2017) 013608.
- [41] S. Gautam, and S.K. Adhikari, *Laser Physics Letters* 12 (2015) 045501.
- [42] R.K. Kumar, V. Lončar, P. Muruganandam, S.K. Adhikari, and A. Balaž, *Comp. Phys. Comm.* 240 (2019) 74; R.K. Kumar, L.E. Young-S, D. Vudragović, A. Balaž, P. Muruganandam, and S.K. Adhikari, *Comp. Phys. Comm.* 195 (2015) 117.
- [43] <http://www.fftw.org/>
- [44] P. Makkar, A. Roy, S. Gautam (2020), "FORTRESS_DATA", Mendeley Data, V1, doi: 10.17632/tct7vjh994.1

Electronic Appendix

This contains the snapshots of the output files, file1.im.dat/file1.re.dat, corresponding to different input parameters.
This data is generated by using FORTRESS.

Started on DAY/MONTH/YEAR, HOURS:MINUTES:SECONDS = 6/ 9/2020, 13:11:36

OPENMP_THREADS = 8, FFTW_THREADS = 8
SWITCH_IM = 1, OPTION_FERRO_POLAR = 1, SWITCH_SOC = 0, GAMMAX = 0.00, TOL = 1.00E-06
Anisotropy ALPHAX = 1.000000, ALPHAY = 20.000000, ALPHAZ = 20.000000

Grid points NX = 2048
Iterations : NITER = 3500000, NSTP = 20000, STP = 4096
Space Step DX = 0.015625
Time Step DT = 0.000024, LX = 32.000000, MAG = 0.500000
OMEGAM = 125.663706, AOSC = 0.2411E-05, C0 = 885.0000, C2 = -4.100000

	Norm	RMS1	RMS2	RMS3	Energy	phi1	phi2	phi3	MAG
Initial:	1.0000	3.6806	3.0052	1.2269	36.14727	0.19607	0.16009	0.06536	0.50000
After NSTP iter.:	0.9941	3.6817	3.0061	1.2272	36.13646	0.19608	0.16010	0.06536	0.50000
After 37603 iter.:	0.9941	3.6818	3.0062	1.2273	36.13646	0.19608	0.16010	0.06536	0.50000

Ended on DAY/MONTH/YEAR, HOURS:MINUTES:SECONDS = 6/ 9/2020, 13:11:53
(a) Time elapsed = 16.733808

Started on DAY/MONTH/YEAR, HOURS:MINUTES:SECONDS = 6/ 9/2020, 19:59:51

OPENMP_THREADS = 8, FFTW_THREADS = 8
SWITCH_IM = 1, OPTION_FERRO_POLAR = 3, SWITCH_SOC = 0, GAMMAX = 0.00, TOL = 1.00E-06
Anisotropy ALPHAX = 1.000000, ALPHAY = 20.000000, ALPHAZ = 20.000000

Grid points NX = 2048
Iterations : NITER = 3500000, NSTP = 600000, STP = 4096
Space Step DX = 0.015625
Time Step DT = 0.000024, LX = 32.000000, MAG = 0.500000
OMEGAM = 125.663706, AOSC = 0.2411E-05, C0 = 885.0000, C2 = -4.100000

	Norm	RMS1	RMS2	RMS3	Energy	phi1	phi2	phi3	MAG
Initial:	1.0000	0.4082	0.4082	0.4082	176.30500	0.43366	0.43366	0.43366	0.00000
After NSTP iter.:	0.9941	3.6816	3.0062	1.2277	36.13646	0.19609	0.16008	0.06534	0.50000
After 737114 iter.:	0.9941	3.6816	3.0063	1.2274	36.13646	0.19609	0.16009	0.06535	0.50000

Ended on DAY/MONTH/YEAR, HOURS:MINUTES:SECONDS = 6/ 9/2020, 20: 7:41
(b) Time elapsed = 470.115744

Figure 1: Contents of 'file1_lim.dat' for ^{87}Rb with (a) OPTION_FERRO_POLAR = 1 and (b) OPTION_FERRO_POLAR = 3 obtained with two runs of 'imretime.spin1_ID.f90'.

Started on DAY/MONTH/YEAR, HOURS:MINUTES:SECONDS = 6/ 9/2020, 20: 3:27

OPENMP_THREADS = 8, FFTW_THREADS = 8
SWITCH_IM = 1, OPTION_FERRO_POLAR = 2, SWITCH_SOC = 0, GAMMAX = 0.00, TOL = 1.00E-06
Anisotropy ALPHAX = 1.000000, ALPHAY = 20.000000, ALPHAZ = 20.000000

Grid points NX = 2048
Iterations : NITER = 3500000, NSTP = 200000, STP = 4096
Space Step DX = 0.015625
Time Step DT = 0.000024, LX = 32.000000, MAG = 0.500000
OMEGAM = 125.663706, AOSC = 0.2411E-05, C0 = 241.0000, C2 = 7.500000

	Norm	RMS1	RMS2	RMS3	Energy	phi1	phi2	phi3	MAG
Initial:	1.0000	0.6124	0.0000	0.3536	48.94655	0.65049	0.00000	0.37556	0.50000
After NSTP iter.:	0.9975	2.9046	0.0000	1.3390	15.32089	0.26941	0.00000	0.18050	0.50000
After 285295 iter.:	0.9975	2.9047	0.0000	1.3388	15.32089	0.26941	0.00000	0.18051	0.50000

Ended on DAY/MONTH/YEAR, HOURS:MINUTES:SECONDS = 6/ 9/2020, 20: 8:10
(a) Time elapsed = 283.236827

Started on DAY/MONTH/YEAR, HOURS:MINUTES:SECONDS = 6/ 9/2020, 20: 2:12

OPENMP_THREADS = 8, FFTW_THREADS = 8
SWITCH_IM = 1, OPTION_FERRO_POLAR = 3, SWITCH_SOC = 0, GAMMAX = 0.00, TOL = 1.00E-06
Anisotropy ALPHAX = 1.000000, ALPHAY = 20.000000, ALPHAZ = 20.000000

Grid points NX = 2048
Iterations : NITER = 3500000, NSTP = 200000, STP = 4096
Space Step DX = 0.015625
Time Step DT = 0.000024, LX = 32.000000, MAG = 0.500000
OMEGAM = 125.663706, AOSC = 0.2411E-05, C0 = 241.0000, C2 = 7.500000

	Norm	RMS1	RMS2	RMS3	Energy	phi1	phi2	phi3	MAG
Initial:	1.0000	0.4082	0.4082	0.4082	49.90235	0.43366	0.43366	0.43366	0.00000
After NSTP iter.:	0.9975	2.9048	0.0048	1.3385	15.32089	0.26940	0.00000	0.18052	0.50000
After 366363 iter.:	0.9975	2.9047	0.0000	1.3388	15.32089	0.26941	0.00000	0.18051	0.50000

Ended on DAY/MONTH/YEAR, HOURS:MINUTES:SECONDS = 6/ 9/2020, 20: 7:48
(b) Time elapsed = 335.719757

Figure 2: Contents of 'file1.im.dat' for ^{23}Na with (a) OPTION_FERRO_POLAR = 2 and (b) OPTION_FERRO_POLAR = 3 obtained with 'imretime_spin1.ID.f90'.

Started on DAY/MONTH/YEAR, HOURS:MINUTES:SECONDS = 6/ 9/2020, 13:29:15

OPENMP_THREADS = 8, FFTW_THREADS = 8
SWITCH_IM = 1, OPTION_FERRO_POLAR = 3, SWITCH_SOC = 1, GAMMAX = 0.50, TOL = 1.00E-06
Anisotropy ALPHAX = 1.000000, ALPHAY = 20.000000, ALPHAZ = 20.000000

Grid points NX = 2048
Iterations : NITER = 10000000, NSTP = 5000000, STP = 4096
Space Step DX = 0.015625
Time Step DT = 0.000024, LX = 32.000000, MAG = 0.000000
OMEGAM = 125.663706, AOSC = 0.2411E-05, C0 = 885.0000, C2 = -4.100000

	Norm	RMS1	RMS2	RMS3	Energy	phi1	phi2	phi3	MAG
Initial:	1.0000	0.4082	0.4082	0.4082	176.30500	0.43366	0.43366	0.43366	0.00000
After NSTP iter.:	0.9941	2.4545	3.4712	2.4545	36.01146	0.13072	0.18486	0.13072	0.00000
After 9547539 iter.:	0.9941	2.4545	3.4712	2.4545	36.01146	0.13072	0.18486	0.13072	0.00000

Ended on DAY/MONTH/YEAR, HOURS:MINUTES:SECONDS = 6/ 9/2020, 14:24:12

(a) Time elapsed = 3296.703670

Started on DAY/MONTH/YEAR, HOURS:MINUTES:SECONDS = 6/ 9/2020, 15: 0:44

OPENMP_THREADS = 8, FFTW_THREADS = 8
SWITCH_IM = 0, OPTION_FERRO_POLAR = 3, SWITCH_SOC = 1, GAMMAX = 0.50, TOL = 1.00E-06
Anisotropy ALPHAX = 1.000000, ALPHAY = 20.000000, ALPHAZ = 20.000000

Grid points NX = 2048
Iterations : NITER = 8000000, NSTP = 5000000, STP = 4096
Space Step DX = 0.015625
Time Step DT = 0.000024, LX = 32.000000, MAG = 0.000000
OMEGAM = 125.663706, AOSC = 0.2411E-05, C0 = 885.0000, C2 = -4.100000

	Norm	RMS1	RMS2	RMS3	Energy	phi1	phi2	phi3	MAG
Initial:	1.0000	2.4545	3.4712	2.4545	36.01146	0.13072	0.18486	0.13072	0.00000
After NSTP iter.:	1.0000	2.4545	3.4712	2.4545	36.01146	0.13072	0.18486	0.13072	0.00000
After 8000000 iter.:	1.0000	2.4545	3.4712	2.4545	36.01146	0.13072	0.18487	0.13072	0.00000

Ended on DAY/MONTH/YEAR, HOURS:MINUTES:SECONDS = 6/ 9/2020, 15:47:48

(b) Time elapsed = 2823.478080

Figure 3: Contents of (a) 'file1.im.dat' and (b) 'file1.re.dat' for ^{87}Rb with non-zero SO coupling strength of 0.5 obtained with 'imretime_spin1_ID.f90'. The realtime simulation corresponds to initial input wavefunctions obtained from the imaginary time run of the code.

Started on DAY/MONTH/YEAR, HOURS:MINUTES:SECONDS = 6/ 9/2020, 13:38:41

OPENMP_THREADS = 8, FFTW_THREADS = 8
SWITCH_IM = 1, OPTION_FERRO_POLAR = 3, SWITCH_SOC = 1, GAMMAX = 0.50, TOL = 1.00E-06
Anisotropy ALPHAX = 1.000000, ALPHAY = 20.000000, ALPHAZ = 20.000000

Grid points NX = 2048
Iterations : NITER = 5000000, NSTP = 3000000, STP = 4096
Space Step DX = 0.015625
Time Step DT = 0.000024, LX = 32.000000, MAG = 0.000000
OMEGAM = 125.663706, AOSC = 0.2411E-05, C0 = 241.0000, C2 = 7.500000

	Norm	RMS1	RMS2	RMS3	Energy	phi1	phi2	phi3	MAG
Initial:	1.0000	0.4082	0.4082	0.4082	49.90235	0.43366	0.43366	0.43366	0.00000
After NSTP iter.:	0.9975	1.5910	2.2624	1.5910	15.12354	0.22944	0.00000	0.22944	0.00000
After 4394547 iter.:	0.9975	1.5924	2.2604	1.5924	15.12354	0.22944	0.00000	0.22944	0.00000

Ended on DAY/MONTH/YEAR, HOURS:MINUTES:SECONDS = 6/ 9/2020, 14:10:18

(a) Time elapsed = 1896.679696

Started on DAY/MONTH/YEAR, HOURS:MINUTES:SECONDS = 6/ 9/2020, 14:59: 8

OPENMP_THREADS = 8, FFTW_THREADS = 8
SWITCH_IM = 0, OPTION_FERRO_POLAR = 3, SWITCH_SOC = 1, GAMMAX = 0.50, TOL = 1.00E-06
Anisotropy ALPHAX = 1.000000, ALPHAY = 20.000000, ALPHAZ = 20.000000

Grid points NX = 2048
Iterations : NITER = 5000000, NSTP = 3000000, STP = 4096
Space Step DX = 0.015625
Time Step DT = 0.000024, LX = 32.000000, MAG = 0.000000
OMEGAM = 125.663706, AOSC = 0.2411E-05, C0 = 241.0000, C2 = 7.500000

	Norm	RMS1	RMS2	RMS3	Energy	phi1	phi2	phi3	MAG
Initial:	1.0000	1.5924	2.2604	1.5924	15.12354	0.22944	0.00000	0.22944	0.00000
After NSTP iter.:	1.0000	1.5924	2.2602	1.5924	15.12355	0.22945	0.00000	0.22945	0.00000
After 5000000 iter.:	1.0000	1.5924	2.2603	1.5924	15.12353	0.22945	0.00000	0.22945	0.00000

Ended on DAY/MONTH/YEAR, HOURS:MINUTES:SECONDS = 6/ 9/2020, 15:27:44

(b) Time elapsed = 1716.413418

Figure 4: Contents of (a) 'file1.im.dat' and (b) 'file1.re.dat' for ^{23}Na with non-zero SO coupling strength of 0.5 obtained with 'imretime-spin1-ID.f90'. The realtime simulations correspond to initial input wavefunctions obtained from the imaginary time run of the code.

Started on DAY/MONTH/YEAR, HOURS:MINUTES:SECONDS = 6/ 9/2020, 14:13:56

OPENMP_THREADS = 16, FFTW_THREADS = 16
SWITCH_IM = 1, OPTION_FERRO_POLAR = 3, SWITCH_SOC = 1, GAMMAX = 0.30, GAMMAY = 0.50, TOL = 1.00E-06
Anisotropy ALPHAX = 1.000000, ALPHAY = 1.000000, ALPHAZ = 20.000000

Grid points NX = 128, NY = 128
Iterations : NITER = 1500000, NSTP = 400000, STP = 200
Space Step DX = 0.100000, DY = 0.100000
Time Step DT = 0.000500, MAG = 0.000000, LX = 12.800000, LY = 12.800000
OMEGAM = 125.663706, AOSC = 0.2411E-05, C0 = 496.442800, C2 = -2.294200

	Norm	RMS1	RMS2	RMS3	Energy	phi1	phi2	phi3	MAG
Initial:	1.0000	0.5774	0.5774	0.5774	40.34338	0.32574	0.32574	0.32574	0.00000
After NSTP iter.:	0.9753	1.6439	1.7506	1.6439	8.34532	0.01984	0.15689	0.01984	0.00000
After 529875 iter.:	0.9754	1.4772	2.0234	1.4772	8.32894	0.07726	0.11616	0.07726	0.00000

Ended on DAY/MONTH/YEAR, HOURS:MINUTES:SECONDS = 6/ 9/2020, 14:30:39

(a) Time elapsed = 1002.63283300

Started on DAY/MONTH/YEAR, HOURS:MINUTES:SECONDS = 6/ 9/2020, 14:18:25

OPENMP_THREADS = 16, FFTW_THREADS = 16
SWITCH_IM = 1, OPTION_FERRO_POLAR = 3, SWITCH_SOC = 1, GAMMAX = 0.30, GAMMAY = -0.60, TOL = 1.00E-06
Anisotropy ALPHAX = 1.000000, ALPHAY = 1.000000, ALPHAZ = 20.000000

Grid points NX = 128, NY = 128
Iterations : NITER = 1500000, NSTP = 100000, STP = 200
Space Step DX = 0.100000, DY = 0.100000
Time Step DT = 0.000500, MAG = 0.000000, LX = 12.800000, LY = 12.800000
OMEGAM = 125.663706, AOSC = 0.2411E-05, C0 = 496.442800, C2 = -2.294200

	Norm	RMS1	RMS2	RMS3	Energy	phi1	phi2	phi3	MAG
Initial:	1.0000	0.5774	0.5774	0.5774	40.34338	0.32574	0.32574	0.32574	0.00000
After NSTP iter.:	0.9754	1.6208	1.7951	1.6208	8.29570	0.00099	0.15932	0.00099	0.00000
After 190667 iter.:	0.9754	1.6208	1.7952	1.6208	8.29569	0.00002	0.15933	0.00002	0.00000

Ended on DAY/MONTH/YEAR, HOURS:MINUTES:SECONDS = 6/ 9/2020, 14:24:28

(b) Time elapsed = 362.88411307

Figure 5: Contents of 'file1_lm.dat' for quasi-2D ^{87}Rb condensate with anisotropic SO coupling strengths of (a) $(\gamma_x, \gamma_y) = (0.3, 0.5)$ and (b) $(\gamma_x, \gamma_y) = (0.3, -0.6)$ obtained with 'imretime_spin1_2D.f90'.

Started on DAY/MONTH/YEAR, HOURS:MINUTES:SECONDS = 6/ 9/2020, 14:26:32

OPENMP_THREADS = 16, FFTW_THREADS = 16
SWITCH_IM = 1, OPTION_FERRO_POLAR = 3, SWITCH_SOC = 1, GAMMAX = 0.60, GAMMAY = 0.00, TOL = 1.00E-06
Anisotropy ALPHAX = 1.000000, ALPHAY = 1.000000, ALPHAZ = 20.000000

Grid points NX = 128, NY = 128
Iterations : NITER = 3500000, NSTP = 30000, STP = 200
Space Step DX = 0.100000, DY = 0.100000
Time Step DT = 0.000500, MAG = 0.000000, LX = 12.800000, LY = 12.800000
OMEGAM = 125.663706, AOSC = 0.2411E-05, C0 = 134.983800, C2 = 4.224200

	Norm	RMS1	RMS2	RMS3	Energy	phi1	phi2	phi3	MAG
Initial:	1.0000	0.5774	0.5774	0.5774	12.04047	0.32574	0.32574	0.32574	0.00000
After NSTP iter.:	0.9871	0.9713	1.6276	0.9713	4.35551	0.15614	0.00011	0.15614	-0.00000
After 49158 iter.:	0.9871	0.9708	1.6282	0.9708	4.35551	0.15614	0.00000	0.15614	0.00000

Ended on DAY/MONTH/YEAR, HOURS:MINUTES:SECONDS = 6/ 9/2020, 14:27:51

(a) Time elapsed = 79.13772297

Started on DAY/MONTH/YEAR, HOURS:MINUTES:SECONDS = 6/ 9/2020, 14:31:37

OPENMP_THREADS = 16, FFTW_THREADS = 16
SWITCH_IM = 1, OPTION_FERRO_POLAR = 3, SWITCH_SOC = 1, GAMMAX = 0.30, GAMMAY = -0.60, TOL = 1.00E-06
Anisotropy ALPHAX = 1.000000, ALPHAY = 1.000000, ALPHAZ = 20.000000

Grid points NX = 128, NY = 128
Iterations : NITER = 1500000, NSTP = 50000, STP = 200
Space Step DX = 0.100000, DY = 0.100000
Time Step DT = 0.000500, MAG = 0.000000, LX = 12.800000, LY = 12.800000
OMEGAM = 125.663706, AOSC = 0.2411E-05, C0 = 134.983800, C2 = 4.224200

	Norm	RMS1	RMS2	RMS3	Energy	phi1	phi2	phi3	MAG
Initial:	1.0000	0.5774	0.5774	0.5774	12.04047	0.32574	0.32574	0.32574	0.00000
After NSTP iter.:	0.9871	1.1669	1.3416	1.1669	4.34266	0.00002	0.22112	0.00002	-0.00000
After 65392 iter.:	0.9871	1.1669	1.3416	1.1669	4.34266	0.00000	0.22112	0.00000	-0.00000

Ended on DAY/MONTH/YEAR, HOURS:MINUTES:SECONDS = 6/ 9/2020, 14:33:38

(b) Time elapsed = 121.15837002

Figure 6: Contents of 'file1.im.dat' for quasi-2D ^{23}Na condensate with anisotropic SO coupling strengths of (a) $(\gamma_x, \gamma_y) = (0.3, 0.5)$ and (b) $(\gamma_x, \gamma_y) = (0.3, -0.6)$ obtained with 'imretime.spin1.2D.f90'.

Started on DAY/MONTH/YEAR, HOURS:MINUTES:SECONDS = 6/ 9/2020, 19:21:36

OPENMP_THREADS = 16, FFTW_THREADS = 16
SWITCH_IM = 1, OPTION_FERRO_POLAR 3, SWITCH_SOC = 1, GAMMAX = 0.50, GAMMAY = 0.50, GAMMAZ = 0.50, TOL = 1.00E-06
Anisotropy ALPHAX = 1.000000, ALPHAY = 1.000000, ALPHAZ = 1.000000

Grid points NX = 128, NY = 128, NZ = 128
Iterations : NITER = 50000, NSTP = 20000, STP = 20
Space Step DX = 0.100000, DY = 0.100000, DZ = 0.100000
Time Step DT = 0.005000, LX = 12.800000, LY = 12.800000, LZ = 12.800000
OMEGAM = 125.663706, AOSC = 0.2411E-05, C0 = 278.2557, C2 = -1.285888

	Norm	RMS1	RMS2	RMS3	Energy	psi1	psi2	psi3	MAG
Initial:	1.0000	0.7071	0.7071	0.7071	10.29745	0.24467	0.24467	0.24467	0.00000
After NSTP iter.:	0.9026	1.2047	1.3139	1.2047	3.75807	0.06856	0.09677	0.06856	0.00000
After 23890 iter.:	0.9026	1.2046	1.3142	1.2046	3.75807	0.06851	0.09684	0.06851	0.00000

Ended on DAY/MONTH/YEAR, HOURS:MINUTES:SECONDS = 6/ 9/2020, 21:23: 1

(a) Time elapsed = 7284.882036

Started on DAY/MONTH/YEAR, HOURS:MINUTES:SECONDS = 6/ 9/2020, 19:22:42

OPENMP_THREADS = 16, FFTW_THREADS = 16
SWITCH_IM = 1, OPTION_FERRO_POLAR 3, SWITCH_SOC = 1, GAMMAX = 0.50, GAMMAY = 0.50, GAMMAZ = 0.50, TOL = 1.00E-06
Anisotropy ALPHAX = 1.000000, ALPHAY = 1.000000, ALPHAZ = 1.000000

Grid points NX = 128, NY = 128, NZ = 128
Iterations : NITER = 50000, NSTP = 10000, STP = 20
Space Step DX = 0.100000, DY = 0.100000, DZ = 0.100000
Time Step DT = 0.005000, LX = 12.800000, LY = 12.800000, LZ = 12.800000
OMEGAM = 125.663706, AOSC = 0.4688E-05, C0 = 75.8013, C2 = 2.439149

	Norm	RMS1	RMS2	RMS3	Energy	psi1	psi2	psi3	MAG
Initial:	1.0000	0.7071	0.7071	0.7071	3.97528	0.24467	0.24467	0.24467	0.00000
After NSTP iter.:	0.9387	1.0887	0.7889	1.0887	2.42376	0.14331	0.00002	0.14331	0.00000
After 10796 iter.:	0.9387	1.0887	0.7889	1.0887	2.42376	0.14331	0.00001	0.14331	0.00000

Ended on DAY/MONTH/YEAR, HOURS:MINUTES:SECONDS = 6/ 9/2020, 20: 7:30

(b) Time elapsed = 2688.591433

Figure 7: Contents of 'file1_im.dat' for (a) a 3D ^{87}Rb and (b) a 3D ^{23}Na condensates with isotropic SO coupling obtained with 'imretime_spin1_3D.f90'.